

Tornadic environments in the Iberian Peninsula and the Balearic Islands based on ERA5 reanalysis

Oriol Rodríguez  | Joan Bech 

Department of Applied Physics –
Meteorology, University of Barcelona,
Barcelona, Spain

Abstract

A dataset of 907 tornado and waterspout events recorded from 1980 to 2018 was built to study convective environments in the Iberian Peninsula and Balearic Islands (western Mediterranean). The events were grouped into different categories, distinguishing waterspouts and tornadoes that were stratified by intensity according to the Fujita (F) scale and the Enhanced Fujita (EF) scale. The analysis separated the north-east (NE) and south-west (SW) subareas in the region of study, which present different seasonal cycles. For each event, atmospheric profiles from the ERA5 reanalysis data were used to determine convective available potential energy (CAPE), storm-relative helicity (SRH), vertical wind-shear (WS), the Universal Tornadic Index (UTI), and the product of wind-shear and the square root of two times CAPE (WMAXSHEAR). Results showed that the NE events are mostly associated with higher CAPE and lower helicity and wind-shear than the SW events. Thus, a significant number of SW tornadoes are associated with high-shear, low-CAPE environments. Moreover, the low-shear, high-LCL tornado environment, which is common inland during warm-season, is more usual in the NE subarea. Composite parameters such as the UTI and WMAXSHEAR₀₆ are good discriminators between significant and weak tornado events, although WMAXSHEAR₀₆ presents some limitations for the SW events due to low CAPE and weak differences in the WS (0–6 km) between the (E)F1 and (E)F2+ events. This weakness was resolved by using the 0–3 km WS instead of the 0–6 km WS when calculating the WMAXSHEAR. A new threshold for WMAXSHEAR₀₃ is proposed ($500 \text{ m}^2\text{-s}^{-2}$) to distinguish between significant and non-significant tornado environments. Finally, the Szilagyi Waterspout Nomogram, originally developed for the Great Lakes of North America, was successfully tested in the forecasting of waterspout formation for the first time in the western Mediterranean area, although the technique should be adapted to correctly detect cool-season mid-latitude waterspouts.

1 | INTRODUCTION

Tornadoes are meteorological phenomena that can produce the strongest natural surface winds on Earth. They are classified at the micro- α or micro- β scale (i.e., characteristic time and horizontal length scales ranging from 1 min to 1 hr and 20 m to 2 km; Orlandi, 1975). Thus, they typically affect small areas and their socioeconomic impact is relatively lower than that of other damaging larger-scale weather events such as floods and windstorms (Gall *et al.*, 2008; Jahn, 2015; Antonescu *et al.*, 2017). Nevertheless, tornado winds can occasionally surpass $100 \text{ m}\cdot\text{s}^{-1}$ (Fujita, 1971; Wakimoto *et al.*, 2015), causing severe damage, injuries and fatalities along their path. Despite recent progress, the precise prediction of their timing and location is still a challenge for operational forecasting systems (Weisman *et al.*, 2015). Due to their high impact and low predictability and given the expected increase in the frequency of severe convective storm environments in the present century (Allen *et al.*, 2014; Seeley and Romps, 2015; Pucik *et al.*, 2017; Viceto *et al.*, 2017), it is necessary to increase our understanding of the environmental conditions that favour tornadogenesis.

During the last decades, several studies have analysed upper-air conditions that favour the development of tornadic storms using proximity sounding data (e.g., Maddox, 1976; Rasmussen and Blanchard, 1998; Groenemeijer and van Delden, 2007; Renko *et al.*, 2016). Finding the most representative sounding for each tornadic event through

proximity criteria (Potvin *et al.*, 2010) enables the calculation of thermodynamic, kinematic and their composite parameters, which can be used to characterize the events depending on their intensity or convective mode.

Some studies have also used numerical model analysis (the Rapid Update Cycle, Rasmussen, 2003) and reanalysis data (ERA-40, Romero *et al.*, 2007; ERA-Interim, Chernokulsky *et al.*, 2019; ERA5, Ingrosso *et al.*, 2020). Results from those studies provide valuable thresholds for different severe weather parameters, which may be useful for weather forecasters to identify potential tornadic storm environments. However, there are some limitations to this approach (i.e., threshold exceedance provides guidance, but must be examined in a global context, considering the presence of all the necessary factors or ‘ingredients’; Doswell and Schultz, 2006).

The use of reanalysis data instead of real atmospheric sounding measurements increases the temporal resolution (normally, only two soundings per day are launched at radiosonde stations) and spatial resolution (the horizontal grid scale of recent reanalysis data such as from ERA5 [C3S, 2017] is around one order of magnitude smaller than the network density of sounding stations in Europe). Therefore, atmospheric profiles from reanalysis usually provide data from a point (latitude, longitude and time) that is closer to the event of interest than a sounding station does. Nevertheless, direct measurements from soundings provide greater vertical resolution than reanalysis and present a more realistic depiction of the atmospheric boundary layer.

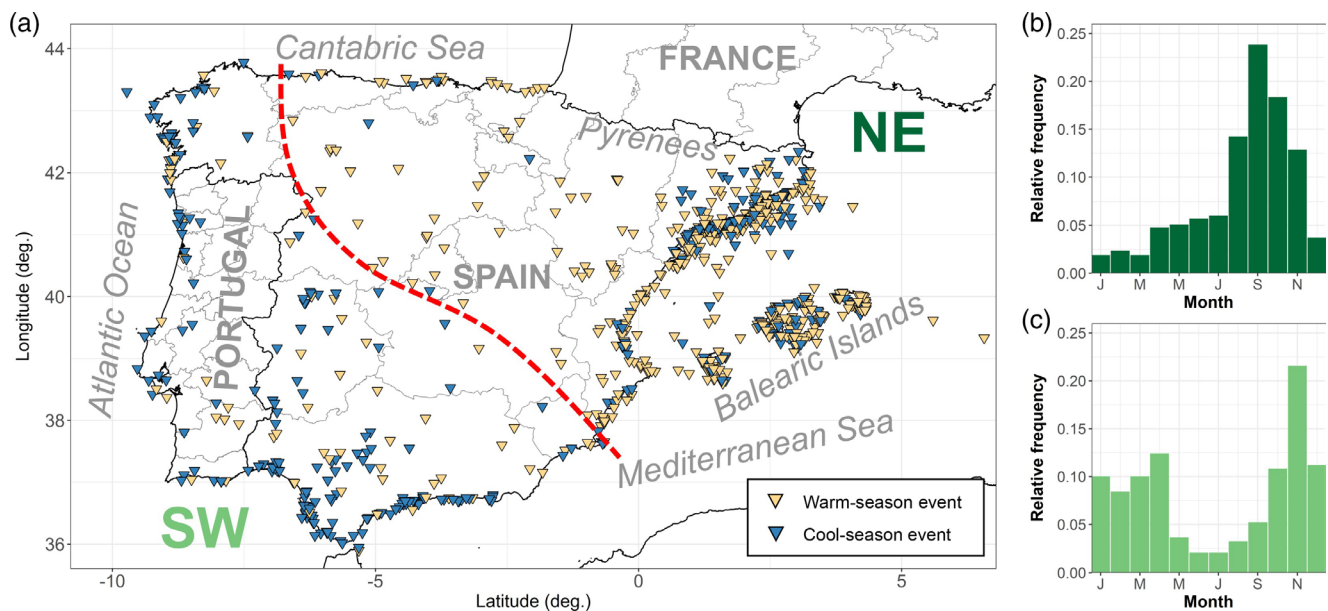


FIGURE 1 (a) Location of the 907 analysed events from 1980 to 2018 on the Iberian Peninsula and Balearic Islands. The dashed line separates the so-called north-east (NE) area, where tornadoes and waterspouts typically occur during warm-season (May–October) and the south-west (SW) area, where they predominate during cool-season (November–April). Relative frequency of tornado and waterspout events in the NE area (b), and the SW area (c) are also shown

These directly affect the calculation of quantities, which are very sensitive to vertical temperature, dew point and wind profile, especially at low levels (Taszarek *et al.*, 2018).

In this article, convective environments prior to tornado formation from events reported in the Iberian Peninsula and Balearic Islands (Figure 1) are characterized. Tornado climatologies of the study area (Leit-ao, 2003; Gayà, 2011, 2018) show that it is regularly affected by tornadoes and waterspouts (i.e., a tornado occurring over a body of water; Glickman and Zenk, 2000). Moreover, it contains some of the spots where tornadoes occur the most frequently in southern Europe (Figure 1a in Antonescu *et al.*, 2017): Balearic Islands, Catalonia (NE Iberia) and the Gulf of Cádiz (SW Iberia). Around 55 million people currently live in this region measuring 630,000 km², where significant tornadic storms occasionally have a substantial social impact, with injuries or even fatalities as well as considerable economic losses (Homar *et al.*, 2003; Bech *et al.*, 2007, 2011; Ramis *et al.*, 2009; Sánchez-Laulhé, 2009; Belo-Pereira *et al.*, 2017; Rodríguez and Bech, 2020).

Despite the scientific literature containing studies on both the tornado climatologies of Spain and Portugal and also a number of detailed tornadic and waterspout case studies, there have been none to date examining the upper-air environments associated with tornadic storms in this region as a whole. Here, we used ERA5 data (C3S, 2017; Hersbach *et al.*, 2020), the latest available reanalysis from the European Centre for Medium-Range Weather Forecasts (ECMWF), which includes tornado and waterspout records occurring in the area from 1980 to 2018. Several thermodynamic, kinematic and composite sounding-derived parameters were calculated from the most representative atmospheric vertical profile for each event. Moreover, we analysed the waterspout distribution in the Szilagyi Waterspout Nomogram (Szilagyi, 2009), which was developed in North America and has already been tested in some European seas, such as the Baltic and the central and eastern Mediterranean (Keul *et al.*, 2009; Sioutas *et al.*, 2013; Renko *et al.*, 2018), but not the western Mediterranean.

The structure of the rest of the article is as follows. In Section 2, tornado and waterspout datasets and the ERA5 reanalysis data are presented, while the parameters calculated from the atmospheric profiles that will be used for further analysis are introduced. In Section 3, results derived from the comparison of the parameter values between the tornado and waterspout events in relation to their intensity are shown and discussed. Finally, in Section 4, conclusions and final remarks are provided, including comments about the potential use of the results in weather surveillance.

2.1 | Tornado and waterspout events database

The tornado and waterspout database used to conduct this study consists of 465 individual tornadoes and 637 individual waterspouts that occurred between 1980 and 2018 in the Iberian Peninsula and Balearic Islands. For all of them, the location (latitude and longitude), date and time of occurrence were considered. If available, the intensity according to the Fujita scale (F-scale; Fujita, 1971) or the Enhanced Fujita scale (EF-scale, WSEC, 2006; Doswell *et al.*, 2009) was also used. If the intensity was unknown, they were recorded as unrated (UR). In this dataset, a waterspout that moved onshore was considered a tornado and was classified according to its damage rating. This accounted for 34% of the tornadoes analysed.

The database was built by merging data from previous publications (Gayà, 2018; Rodríguez and Bech, 2018, hereafter referred to as RB18) and incorporating information from citizen collaborative platforms. These platforms included the European Severe Weather Database (ESWD, from the European Severe Storm Laboratory, ESSL; Dotzek *et al.*, 2009), the Reporting System of Singular Atmospheric Observations (SINOBAS, from the Spanish Meteorological Agency, AEMET; Gutiérrez *et al.*, 2015) and the Meteorological Spotters Network (XOM, from the Meteorological Service of Catalonia, SMC; Ripoll *et al.*, 2016). Only confirmed cases, according to quality control from the original databases (i.e., QC1 and QC2 for the ESWD reports, Groenemeijer *et al.*, 2017), were considered. These data were also complemented with other tornado and waterspout reports from the media and social networks, which have become increasingly important in recent years (Hyvärinen and Saltikoff, 2010). Thus, a sample of 1,102 individual cases was collected, after discarding 320 cases due to quality control.

It is well known that on some occasions, several tornadoes or waterspouts (here referred to simply as vortices) may form in a relatively short time window from the same convective storm or cloud system (Dowell and Bluestein, 2002; Bech *et al.*, 2007; Sioutas *et al.*, 2013). As mentioned above, the main goal of this study was to analyse environmental conditions from individual cases. However, to avoid the overrepresentation of specific meteorological situations, an event was considered unique when:

1. two or more vortices occurred within 50 km.
2. the time elapsed among them was less than 2 hours.

Moreover, in the case of multiple vortices that formed offshore and inland, they were considered as only one tornado event. As a result, 426 tornado and 481 waterspout events were analysed.

Tornadoes can be formed in different environments depending on the convective mode (e.g., supercells or mesoscale convective systems; see, for example, Agee and Jones (2009), Grams *et al.* (2012), Markowski and Richardson, (2009), Thompson *et al.* (2012, 2013)). For instance, mesocyclonic tornadoes require high-shear environments, whereas those spawned by multicells are usually associated with low-shear environments. Therefore, it would be ideal to classify the analysed events according to the parent-convective cell type to avoid compensations in the parameter values. However, there are several limitations to the radar data collected from the region of study (see Quirantes *et al.*, 2014 for further details), specifically with the data concerning the first half of the analysed period. The Spanish radar network was not completed until late 2007, with the radar on the Balearic Islands the last one to be put into operation. As these islands are where tornadoes occur the most frequently in the study region (together with Catalonia), it would not be possible to make the complete convective mode analysis for a substantial number of the tornado events studied here. Following similar previous studies (Craven and Brooks, 2004; Púčik *et al.*, 2015; Ingrassio *et al.*, 2020), the 426 tornadic events were clustered according to their intensity, which was estimated using the F-scale or the EF-scale, into the categories (E)F0, (E)F1, (E)F2+ (i.e., F2/EF2 or stronger) and UR (unrated). In these categories, (E) indicates the use of the EF-scale and F the F-scale. On the other hand, waterspout events were grouped into a single category (WAT) (Table 1).

When analysing the monthly distributions of the tornadoes and waterspouts, two different subregions became apparent (Figure 1): the north-east of the Iberian Peninsula and the Balearic Islands (NE), and the south-west of the Iberian Peninsula (SW). In the NE, events occur more frequently during the warm-season (72.9% from May to October), similar to other Mediterranean countries such

as Italy (Miglietta and Matsangouras, 2018), while in the SW, the events are more common during the cool-season (73.3% from November to April). These differences in seasonal distribution are a consequence of synoptic configurations that favour deep moist convection and tornado formation in both areas. Tornadoes in the SW are mostly associated with cool-season Atlantic fronts, whereas the tornadic synoptic situations in the NE are usually associated with the inland diurnal heating cycle during the warm-season and the Mediterranean thermodynamic instability that is typical from late summer and autumn (Riesco *et al.*, 2015). Therefore, in this paper, these two different areas were studied separately.

The number of reported events is significantly higher in the NE than in the SW (Figure 1 and Table 1). Gayà (2018) and Antonescu *et al.* (2017) pointed out that the Mediterranean slope of the Iberian Peninsula and the Balearic Islands are the most frequently affected by tornadoes in the study region. The moister and relatively warm marine boundary layer of that area increases low-tropospheric instability and makes environmental conditions more favourable to deep convection (Miglietta *et al.*, 2017), which is also consistent with the spatial and temporal distribution of lightning events (Taszarek *et al.*, 2019). This has been highlighted by the exhaustive monitoring of tornadoes and waterspouts in Catalonia and the Balearic Islands during the last three decades by several studies (Gayà *et al.*, 2001; Gayà, 2011; Arús, 2018; Rodríguez *et al.*, 2020). This may explain the higher detection of non-damaging or weakly-damaging events such as waterspouts and (E)F0 tornadoes in this subarea, in contrast to the rest of the Iberian Peninsula where the ratio of these types of events is much lower.

2.2 | ERA5

Vertical temperature, dew point and wind profiles from each tornado and waterspout event contained in the database were retrieved from the ECMWF ERA5 reanalysis (C3S, 2017), whose spatial and temporal resolution are

TABLE 1 Number of individual vortices (tornadoes and waterspouts), number of atmospheric profiles and number of NE and SW profiles analysed for each category considering (Enhanced) Fujita scale intensities (E)F0, (E)F1, (E)F2+, unrated tornadoes (UR) and waterspouts (WAT)

Category	Number of individual vortices	Number of profiles	Number of NE profiles	Number of SW profiles
(E)F0	211	196	128	68
(E)F1	185	166	64	102
(E)F2+	47	44	30	14
UR	22	20	10	10
WAT	637	481	424	57

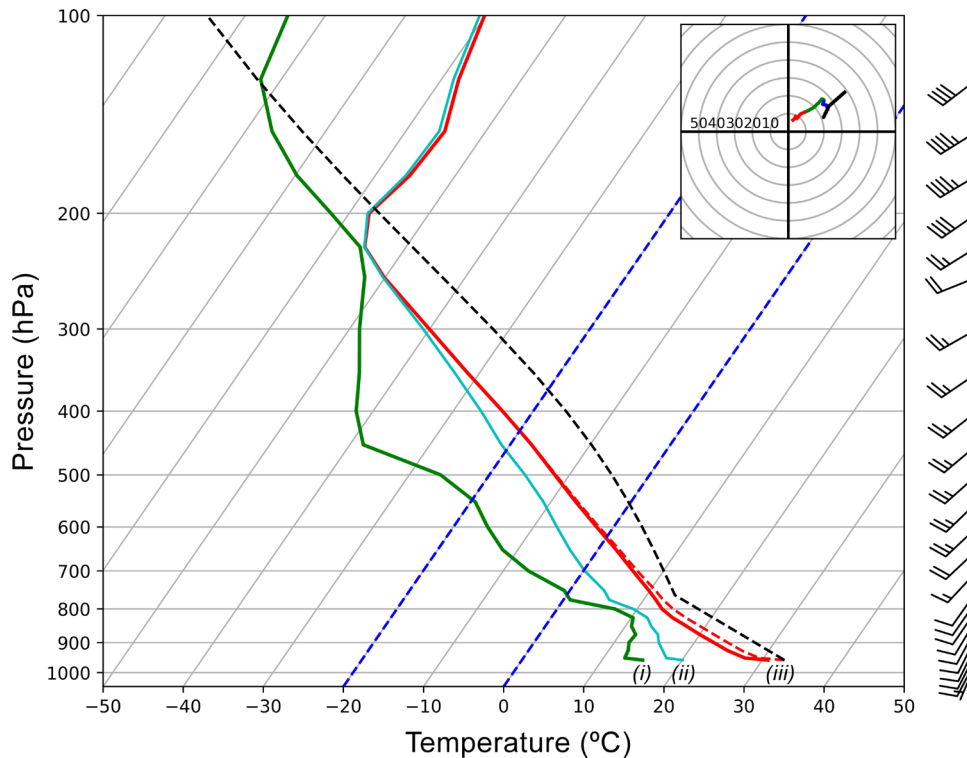


FIGURE 2 Skew T – logp diagram for l'Espluga de Francolí (Catalonia) tornado of 31st August 1994 at 1445 UTC (41.39°N, 1.11°E). ERA5 reanalysis data from 14 UTC August 31, 1994 and 41.50°N, 1.00°E grid point has been used to analyse this case and Sounding and Hodograph Analysis and Research Program in Python (SHARPPy), from Blumberg *et al.* (2017), has been used to plot the diagram. Profiles plotted include dew point (solid line (i)), wet-bulb temperature (solid line (ii)) and temperature (solid line (iii))

0.25° and 1 hr, respectively, with data available on 37 pressure levels and surface. The most representative sounding of an event was considered, that is, the vertical profile from the closest grid point and immediately prior to touchdown of the analysed case, with this point being offshore for waterspouts even if there was landfall. Figure 2 shows the sounding selected to describe the 1994 tornado in l'Espluga de Francolí in Catalonia (Ramis *et al.*, 1997) as an example. Therefore, 907 soundings were analysed (Table 1).

2.3 | Parameters analysed

The selection of the thermodynamic and kinematic parameters to be analysed was based on similar previous studies (e.g., Craven and Brooks, 2004; Groenemeijer and van Delden, 2007; Kaltenböck *et al.*, 2009). Therefore, convective available potential energy (CAPE), convective inhibition (CIN), storm-relative helicity (SRH) and wind-shear (WS) were studied to characterize severe storm environments (Table A1 in Appendix A). Moreover, composite parameters (i.e., a combination of the above-mentioned parameters) were also investigated to assess

favourable environments for tornadic storms. Taszarek and Kolendowicz (2013) proposed the Universal Tornadoic Index (UTI) to distinguish between tornadic and non-tornadic environments in Poland. As shown in Table A1, the UTI takes into account low-level humidity, instability and shear, which are required for tornadic storms, as discussed previously (Rasmussen and Blanchard, 1998; Grams *et al.*, 2012). RB18 demonstrated that the UTI could distinguish non-tornadic thunderstorms from EF1 or stronger cases in Catalonia. Several studies have recently assessed the behaviour of the product of WS and the square root of two times CAPE (WMAXSHEAR) to identify significant tornado environments (Taszarek *et al.*, 2017; Chernokulsky *et al.*, 2019). Therefore, these two composite parameters were also analysed in this study, with the aim of testing them with data from the Iberian Peninsula and Balearic Islands.

Calculations of the thermodynamic and kinematic parameters were carried out using Sounding and Hodograph Analysis and Research Program in Python (SHARPPy; Blumberg *et al.*, 2017). CAPE and CIN were calculated using the virtual temperature correction (Doswell and Rasmussen, 1994) and the most-unstable

air parcel. This parcel allows the assessment of convection when it does not develop from near-surface air, but from a higher level. This is common in nocturnal convection, where the surface-air is cooler than at higher altitudes (Groenemeijer *et al.*, 2019). Moreover, most-unstable CAPE has been used in other studies to investigate environments favourable to tornadic storms (Púček *et al.*, 2015; Renko *et al.*, 2016; Ingresso *et al.*, 2020).

SRH was calculated for the 0–3 km (SRH_{03}) and 0–1 km (SRH_{01}) layers. Storm-motion vector, which is required to calculate SRH (Table A1), was estimated with the Bunkers method (Bunkers *et al.*, 2000), which is used by SHARPPy. WS was calculated for the deep (0–6 km, WS_{06}), middle (0–3 km, WS_{03}) and low (0–1 km, WS_{01}) layers, and WMAXSHEAR for the 0–6 km ($WMAXSHEAR_{06}$) and 0–3 km ($WMAXSHEAR_{03}$) layers. All these layers are defined as above ground level (AGL).

The Kolmogorov–Smirnov (KS) test was carried out to assess significant differences among the categories for each parameter and to compare the distributions of each parameter between the NE and SW events. The results of this test are shown in Tables B1 and B2 (Appendix B).

Finally, the convective cloud depth (CCD) was calculated for waterspout events, that is, the difference between the equilibrium level (EL) and the lifting condensation level

(LCL), also using the most-unstable air parcel. Data on the sea surface temperature (SST), and the 850 hPa temperature (T_{850}) and wind speed (W_{850}) for each waterspout event were directly provided by the ERA5 reanalysis. All these data were used to analyse waterspout distribution on the Szilagyí Waterspout Nomogram (Szilagyí, 2009).

3 | RESULTS AND DISCUSSION

In this section, results from the parameter analysis are presented and discussed in three subsections: thermodynamic parameters (CAPE and CIN), kinematic parameters (SRH and WS) and composite parameters (UTI, WMAXSHEAR, the relationship between CAPE and WS_{03} , and the Szilagyí Waterspout Nomogram).

3.1 | Thermodynamic parameters

3.1.1 | Convective available potential energy

CAPE presents substantial differences for each category between the NE and SW regions (Figure 3a,b). CAPE has

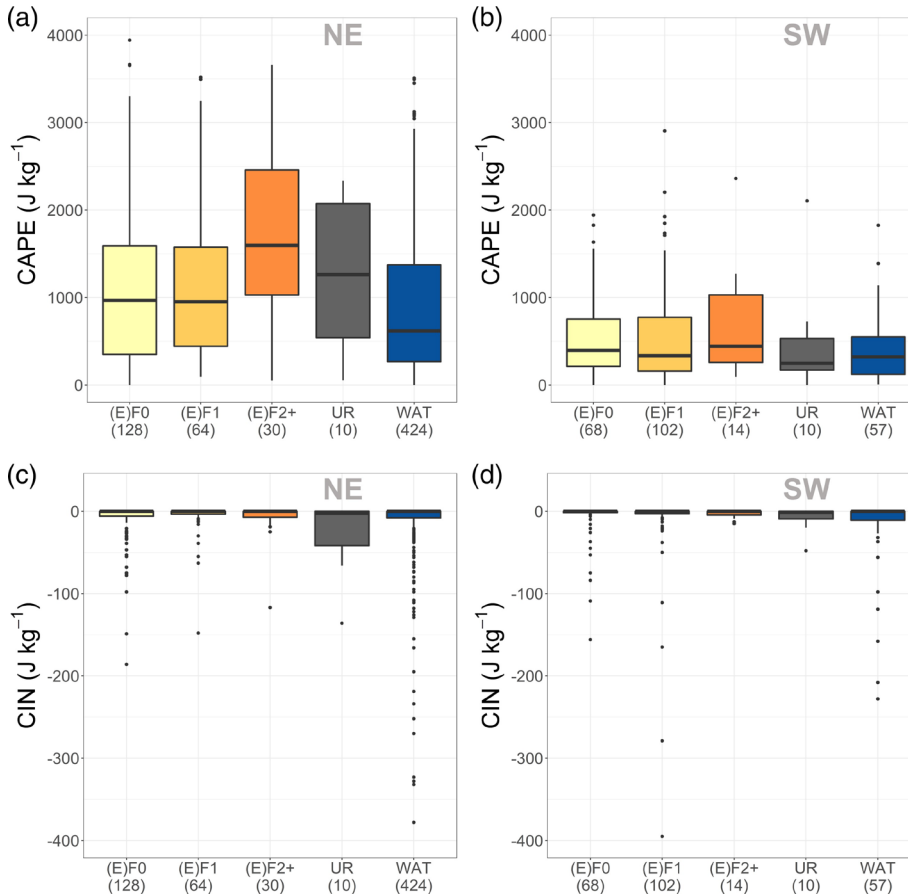


FIGURE 3 CAPE boxplots for NE events (a) and SW events (b), and for CIN for NE (c) and SW (d) events showing 25th, 50th and 75th percentiles. Whiskers extend from 25th and 75th percentiles to minimum and maximum values, respectively, unless these exceed 1.5 times the inter-quartile range. Then, outliers are presented as points above or below whiskers. The number of analysed vertical profiles of each sounding type is shown in brackets below the boxplot category name including rated tornadoes ((E)F0, (E)F1, (E)F2+), unrated tornadoes (UR) and waterspout (WAT) events

a wide range of values for the NE events, usually being higher than those for the SW events. As explained in Section 2.1, most of the SW cases occur during the cool-season, when surface specific humidity is lower than in the warm-season, thereby favouring low CAPE (as discussed by Riemann-Campe *et al.*, 2009). The small number of warm-season tornadic events in the SW favour low CAPE and a smaller CAPE range, which is consistent with the findings of previous studies (Matsangouras *et al.*, 2017; Childs *et al.*, 2018).

Weak tornadic events (i.e., (E)F0 and (E)F1) present similar CAPE, with a median of around 950 J kg^{-1} for the NE events and 370 J kg^{-1} for the SW events. On the other hand, significant tornadic events ((E)F2+) tend to present higher values than the rest of the sounding types, with statistically significant differences for the NE events (Table B1). By contrast, the differences are not statistically significant for the events in the SW subregion, although the median for the (E)F2+ events is slightly higher than that for the weak cases.

WAT are associated with similar or slightly lower CAPE compared to that for weak tornadoes in both regions, as reported previously (Gayà *et al.*, 2001; Kahraman *et al.*, 2017). However, the 50th percentile for the NE WAT is 618 J kg^{-1} , comparable to that reported by Renko *et al.* (2016), and 321 J kg^{-1} for the SW, which is similar to the results from other colder seaways (e.g., Groenemeijer and van Delden [2007], who studied tornadic upper-air conditions in the Netherlands).

Here, CAPE values are generally smaller than those presented in the studies on US tornadic events (Thompson *et al.*, 2012), but similar to those reported in studies performed in Europe (Groenemeijer and van Delden, 2007; Pucik *et al.*, 2015). The combination of steep lapse rates developing over the Rocky Mountains and very low-level moist-air from the Gulf of Mexico produces higher-CAPE environments in the United States than in Europe. Therefore, whereas tornadoes can be associated with a large range of CAPE in the United States, they are usually related to lower CAPE values in Europe (Grünwald and Brooks, 2011).

3.1.2 | Convective inhibition

WAT events in both the NE and SW regions present the largest CIN (more negative), despite the UR events in the NE, probably due to the small sample size (Figure 3c,d). The 25th percentile is -8 J kg^{-1} for the NE WAT, surpassing -200 J kg^{-1} in several cases, and -11 J kg^{-1} for the SW WAT. These results are similar to those presented in Renko *et al.* (2016). It is remarkable that whereas only

1–4% of the (E)F0, (E)F1 and (E)F2+ tornado events are associated with CIN surpassing -100 J kg^{-1} , this percentage rises up to 6–7% for WAT. Nevertheless, there is a considerable overlap between the distributions. In summary, CIN does not exhibit statistically significant differences between the categories (Table B1) or between the NE and SW subregions (Table B2).

The greater CIN associated with WAT events might be related to the shallow stable layer that forms just over the sea surface when a warm air mass is advected. Thus, the dew point approaches the SST, resulting in high CAPE that is often highly capped with high CIN (Groenemeijer *et al.*, 2019). A mechanism to force the lifting to initiate convection is required, particularly in these cases.

3.2 | Kinematic parameters

3.2.1 | Storm-relative helicity

SRH quantifies the potential for cyclonic updraft rotation in right-moving supercells (Davies-Jones *et al.*, 1990). Thus, environments characterized by high SRH usually support the formation of mesocyclones and tornadoes (Rasmussen and Blanchard, 1998; Thompson *et al.*, 2003). More specifically, SRH_{01} accounts for the possible existence of large low-level horizontal vorticity, which plays a very important role in tornadogenesis (Wade *et al.*, 2018).

As shown in Figure 4, SRH presents higher values for all the SW tornado categories (Figure 4b,d) than for the NE ones (Figure 4a,c). This is consistent with the occurrence of SW tornadoes during the cool-season, which usually presents high-shear, low-CAPE (HSLC) environments (Sherburn and Parker, 2014), as shown in Table 2. This is also in accordance with the low CAPE mentioned above. In these situations, tornadoes are usually formed within low-topped mini-supercells or in quasi-linear convective system mesovortices (Thompson *et al.*, 2012; Davis and Parker, 2014).

Tornado formation has been observed occasionally in environments with low helicity ($\text{SRH}_{01} < 75 \text{ m}^2 \text{ s}^{-2}$) and/or high LCL ($> 1,300 \text{ m}$), the so-called LHLCL environments (Davies, 2006). These conditions, which are more usual inland during the warm-season and are therefore more common in the NE atmospheric profile samples (Table 2), may contribute to the decreased SRH percentiles for the NE events. As an example, the vertical profile shown in Figure 2, which corresponds to the l'Espluga de Francolí (Catalonia) tornado of 31st August 1994, presents similarities to the high-based tornadic environments reported in Davies (2006).

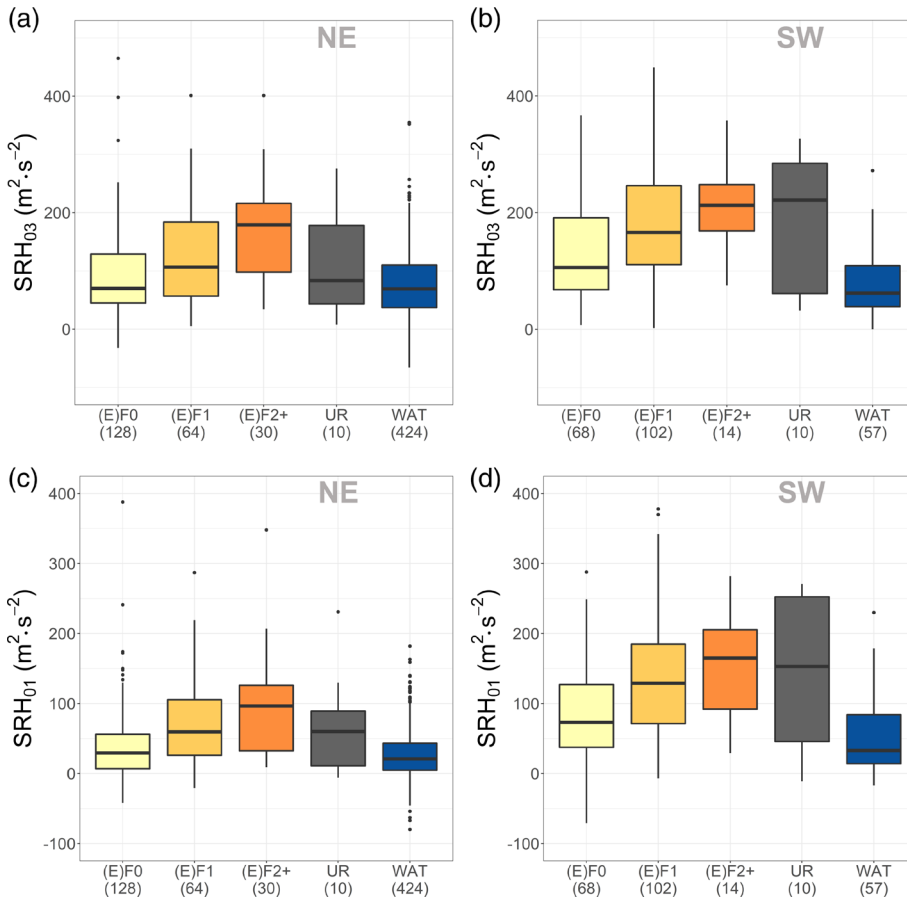


FIGURE 4 As Figure 3, but for SRH_{03} for NE (a) and SW (b), and for SRH_{01} for NE (c) and SW (d)

TABLE 2 Number of warm-season, cool-season, high-shear, low-CAPE (HSLC) and low-helicity, high-LCL (LHHLCL) soundings for NE tornado (NE-TOR), NE waterspout (NE-WAT), SW tornado (SW-TOR) and SW waterspout (SW-WAT) sounding groups

Sounding group	Warm-season (over total)	Cool-season (over total)	HSLC			LHHLCL (over total)	LHHLCL (over warm-season)	LHHLCL (over cool-season)
			(over total)	HSLC (over warm-season)	HSLC (over cool-season)			
NE-TOR	169 (73%)	63 (27%)	31 (13%)	14 (8%)	17 (27%)	31 (13%)	29 (17%)	2 (3%)
NE-WAT	309 (73%)	115 (27%)	75 (18%)	39 (13%)	36 (31%)	7 (2%)	4 (1%)	3 (3%)
SW-TOR	55 (28%)	139 (72%)	85 (44%)	9 (16%)	76 (55%)	11 (6%)	10 (18%)	1 (1%)
SW-WAT	12 (21%)	45 (79%)	15 (26%)	2 (17%)	13 (29%)	1 (2%)	1 (8%)	0 (0%)

Note: In brackets, the percentage over the sample data indicated is shown. Note that HSLC environment is defined by $SBCAPE \leq 500 \text{ J}\cdot\text{kg}^{-1}$, $MUCAPE \leq 1,000 \text{ J}\cdot\text{kg}^{-1}$, and $WS_{06} \geq 18 \text{ m}\cdot\text{s}^{-1}$, and LHHLCL is defined by $SRH_{01} < 75 \text{ m}^2\cdot\text{s}^{-2}$ and $LCL > 1,300 \text{ m}$.

In Figure 4, a clear positive correlation can be seen between helicity and tornado intensity: the higher the SRH, the stronger the tornado can be. This is consistent with previous studies such as Groenemeijer and van Delden (2007) and Taszarek and Kolendowicz (2013). However, the helicity values found here are smaller than those reported in the other two studies, especially for the NE cases. This could be due to a higher fraction of non-mesocyclonic tornadoes (Markowski and Richardson, 2009; Thompson *et al.*, 2012), given that 34% of the tornadoes analysed in this study were formed offshore.

WAT events are commonly associated with weak environmental helicity, as explained in Sioutas and Keul (2007) and Renko *et al.* (2016). SRH_{03} is usually between 35 and $110 \text{ m}^2\cdot\text{s}^{-2}$, and SRH_{01} between 10 and $85 \text{ m}^2\cdot\text{s}^{-2}$.

It is remarkable that for the NE tornado events, the SRH values of the UR cases overlap with those of the (E) F0 and (E)F1 tornadoes, but are smaller than those of the (E)F2+ cases, which is consistent with the observations of Grünwald and Brooks (2011). By contrast, for the SW tornado events, the SRH_{03} and SRH_{01} of the UR events

are comparable to those of all the other categories, including the (E)F2+ cases. This suggests the possible presence of significant tornadoes in the SW UR class.

In RB18, the thresholds $SRH_{03} > 150 \text{ m}^2 \text{ s}^{-2}$ and $SRH_{01} > 70 \text{ m}^2 \text{ s}^{-2}$ were proposed to distinguish between (E)F1+ tornadoes and non-tornadic storms. Here, 40% of the NE (E)F1+ tornadoes and 58% of the SW (E)F1+ events surpass the SRH_{03} threshold, while 47% of the NE (E)F1+ tornadoes and 76% of the SW (E)F1+ events exceed the SRH_{01} threshold. These values were also surpassed by the majority of the tornadic events analysed in Thompson *et al.* (2003), which were supercell-related.

Nevertheless, it should be noted that these SRH thresholds can generate a high number of false alarms when used to detect tornadic environments. Furthermore, most of the non-severe events studied in Groenemeijer and van Delden (2007) had an SRH_{01} between 11 and $97 \text{ m}^2 \text{ s}^{-2}$.

3.2.2 | Wind-shear

WS presents similar trends as the SRH, showing a positive correlation with tornado intensity. This is consistent

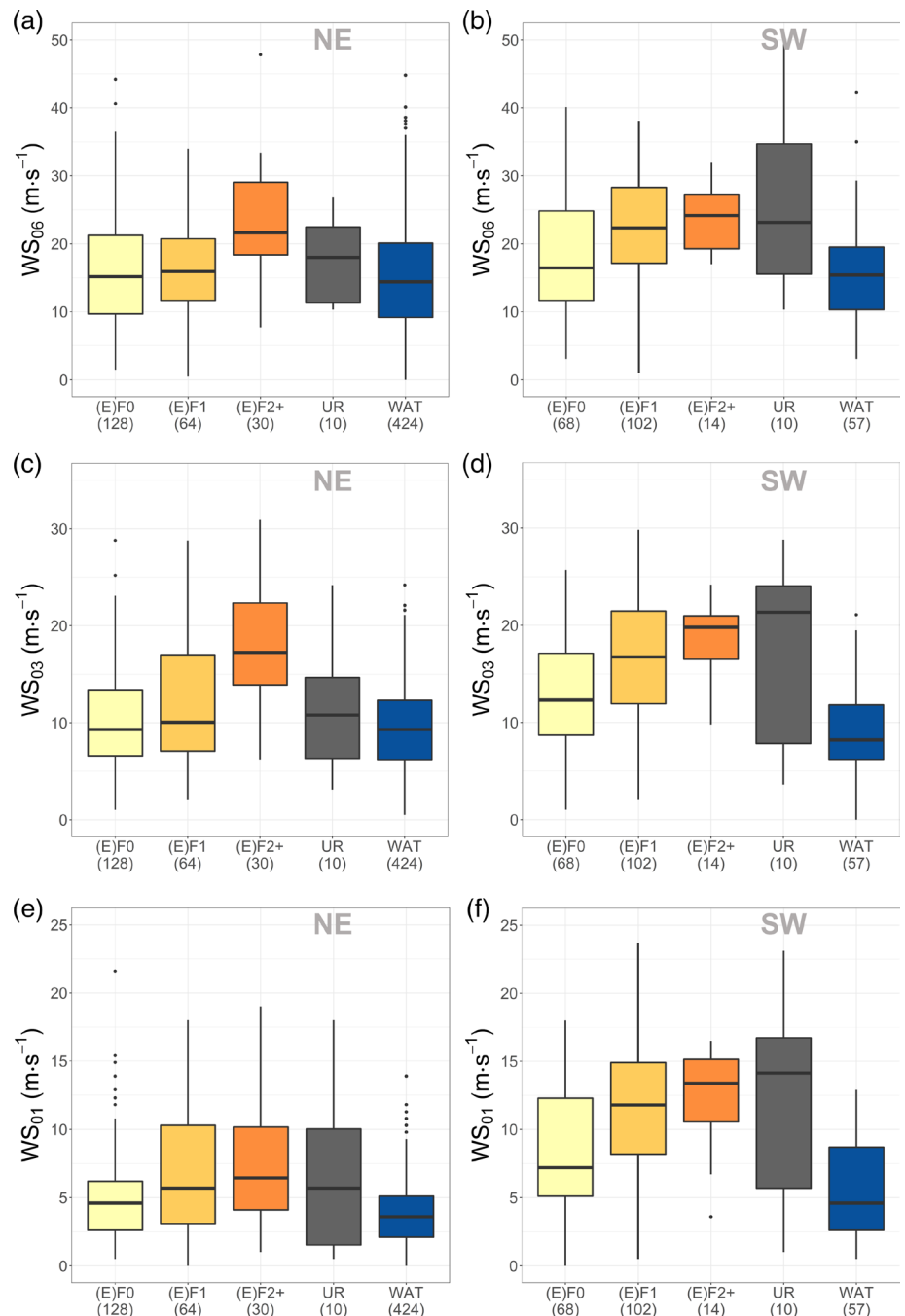


FIGURE 5 As Figure 3, but for WS_{06} for NE (a) and SW (b), for WS_{03} for NE (c) and SW (d), and for WS_{01} for NE (e) and SW (f)

with the fact that WS and SRH are dependent on each other (see Weisman and Rotunno, 2000 for further discussion). Therefore, the significant tornadoes in our dataset are usually associated with stronger WS compared to weak tornadoes and WAT (Figure 5), which is consistent with previous studies (e.g., Monteverdi *et al.*, 2003; Groenemeijer and van Delden, 2007). However, although the median WS of the (E)F2+ SW events is higher than that of the (E)F1 tornadoes (Figure 5b,d,f), there are no statistically significant differences between these two categories (Table B1). By contrast, the NE events (Figure 5a,c,e) show significant differences between the (E)F1 and (E)F2+ tornadoes for WS_{06} and WS_{03} , but not for WS_{01} . The WS for UR events follows a similar pattern as the helicity. Thus, whereas the UR and weak tornadoes have comparable WS in the NE, the WS for the UR events is also similar to that of the (E)F2+ tornadoes in the SW.

There are statistically significant differences in WS between the NE and SW subregions for all the analysed layers due to the monthly distribution of the tornado events. WS is higher for the SW events than the NE ones, which is consistent with the helicity and CAPE results.

This shows the predominance of HSLC environments for the events occurring during the cool-season and, therefore, in the south-west of the Iberian Peninsula (Table 2).

Previous studies have indicated that environments with $WS_{06} > 20 \text{ m-s}^{-1}$ are associated with the occurrence of significant tornadoes (Weisman and Klemp, 1982; Thompson *et al.*, 2003, 2012; Grams *et al.*, 2012; Ingrosso *et al.*, 2020). These tornadoes usually have a mesocyclonic origin (Markowski and Richardson, 2009). Almost 63% of the NE and 71% of the SW (E)F2+ events surpass the above-mentioned WS_{06} threshold (Figure 5a, b). The 50th percentile is 21.6 m-s^{-1} for the NE events and 24.2 m-s^{-1} for the SW cases, which are similar to those reported by Taszarek and Kolendowicz (2013) and Chernokulsky *et al.* (2019).

Taszarek *et al.* (2017) and RB18 pointed out that WS_{03} is a good discriminator between (E)F1+ tornadoes and non-tornadic storms (see Appendix C). WS_{03} greater than 15 m-s^{-1} is usually associated with environments that favour tornadoes, especially the significant ones. Here, 48% of the NE and 66% of the SW (E)F1+ events exceed this value, although the percentage is higher for the (E)F2+ cases from both subregions (more than 70% of all the significant events), as shown in Figure 5c,d.

WS_{01} presents the most significant differences between the NE and SW subregions (Figure 5e,f). In the NE, the median WS_{01} is 4.6 m-s^{-1} for weak events (considering the (E)F0 and (E)F1 categories together) and 6.4 m-s^{-1} for significant events. In the SW, the corresponding medians are 10.6 and 13.0 m-s^{-1} ,

respectively. The values for the SW tornado environments are similar to those of the other studies performed in Europe (Groenemeijer and van Delden, 2007; Taszarek and Kolendowicz, 2013). By contrast, the values for the NE tornado profiles are 30–50% smaller, probably due to the monthly distribution of the tornadic events. In fact, only 40% of the significant tornado environments in the NE exceed 8 m-s^{-1} , a threshold proposed in RB18, whereas 79% of the SW (E)F2+ events surpass this threshold. The seasonal dependence of WS observed for the significant events is also reported in Ingrosso *et al.* (2020), where the lowest values for (E)F2+ tornadoes in Italy occur during the spring and summer, and the highest in autumn.

Waterspouts are commonly associated with weak-shear environments (Keul *et al.*, 2009; Sioutas *et al.*, 2013). For all the atmospheric layers analysed, WAT category presents the lowest medians, with the differences between the NE and SW events not being statistically significant for the 0–6 km and the 0–3 km layers (Table B2). Similar results have been reported for other European regions (Groenemeijer and van Delden, 2007; Renko *et al.*, 2016) and the Florida Keys in the USA (Devanas and Stefanova, 2018).

3.3 | Composite parameters

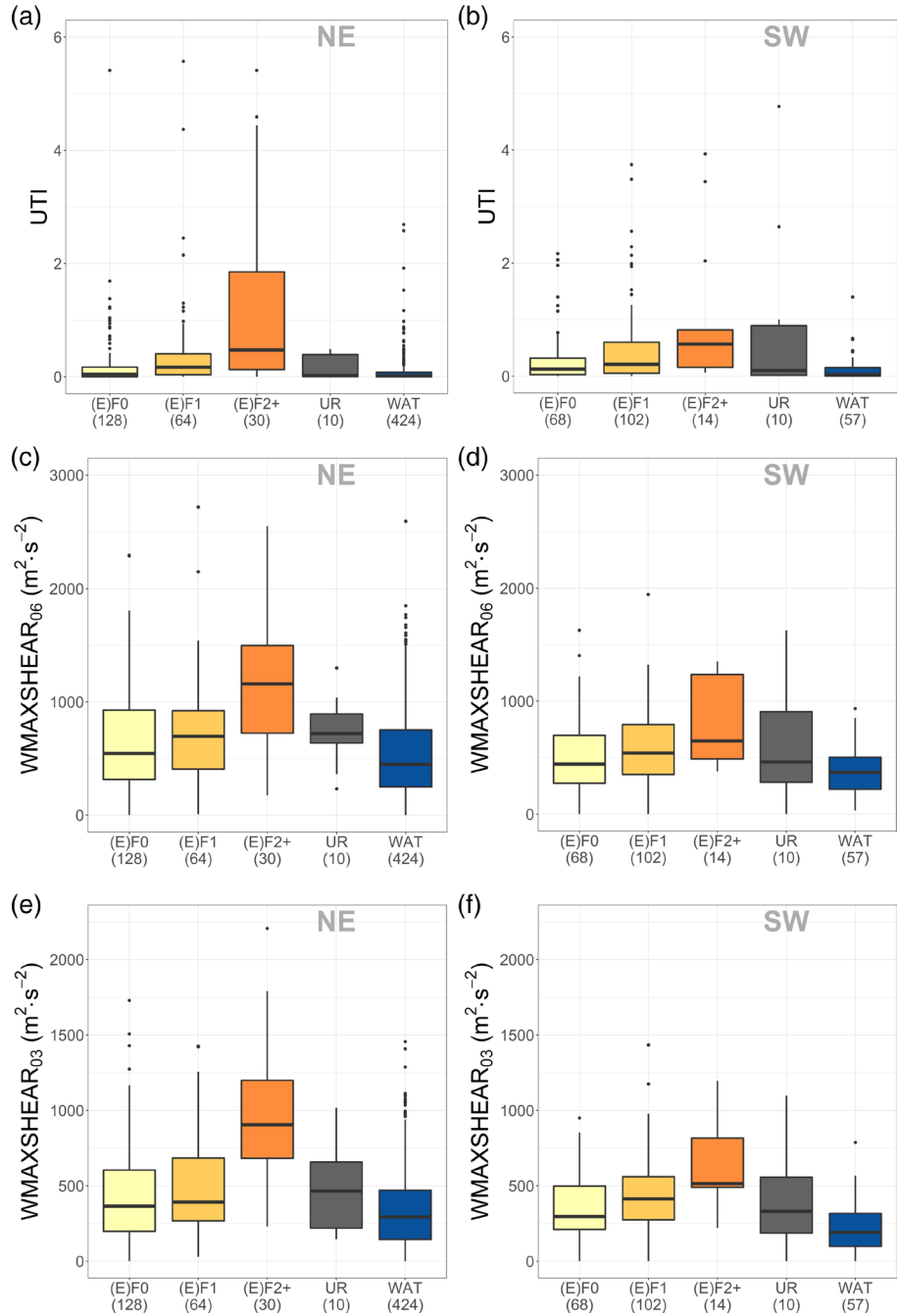
3.3.1 | Universal tornadic index

The UTI, originally proposed by Taszarek and Kolendowicz (2013), was used in Catalonia by RB18 to successfully distinguish between non-tornadic thunderstorms and (E)F1+ tornado-related environments, with the UTI exceeding 0.3 for the latter. In the present study, 21% of the (E)F0 events, 40% of the (E)F1 cases, 66% of the (E)F2+ tornadoes, 40% of the UR cases and 9% of the WAT events from the whole dataset surpass this threshold.

According to its definition (see Table A1), $UTI = 0$ when $LCL > 1,500 \text{ m}$. Therefore, for LHHCL environments (such as the example shown in Figure 2, where the LCL is $1,950 \text{ m}$), this parameter is not useful in detecting a potential tornado environment. Thus, as explained in detail in Davies (2006), other elements have to be examined to assess the potential of tornado formation in LHHCL environments, such as high low-level lapse-rates, high CAPE in the 0–3 km layer, and small CIN (not shown).

Significant tornadoes are usually associated with a higher UTI than weak tornadic events (see Figure 6a,b). A positive correlation between the UTI and tornado intensity can be inferred from the percentiles of this

FIGURE 6 As Figure 3, but for UTI for NE (a) and SW (b), for WMAXSHEAR₀₆ for NE (c) and SW (d), and for WMAXSHEAR₀₃ for NE (e) and SW (f)



parameter for each category. The median is around 0.05 for (E)F0 cases (in both the NE and SW subregions), 0.20 for (E)F1 tornadoes and 0.50 for (E)F2+ events. These values are smaller than those presented in Taszarek and Kolendowicz (2013), mainly because kinematic low-level parameters (i.e., WS₀₁ and SRH₀₁) are also smaller in the study area. Nevertheless, our results are similar to the median UTI reported by RB18.

There are no significant differences in the UTI between the NE and SW events, except for the (E)F0

cases (Table B2). Therefore, this parameter can also detect warm-season and cool-season tornadic events, in contrast to the parameters analysed previously. Moreover, the UTI can distinguish between the (E)F0, (E)F1, (E)F2+ and WAT sounding types ($p < .080$), although the KS-test results show that the differences between the (E)F1 and (E)F2+ tornadoes for the SW are not statistically significant (Table B1). Furthermore, whereas the UR and weak events have a similar UTI in the NE cases, the UTI for the UR events is also comparable to that of the

significant events in the SW data, similar to that found for the kinematic parameters.

3.3.2 | WMAXSHEAR

WMAXSHEAR₀₆ was used in Taszarek *et al.* (2017) to assess thunderstorm severity and in Chernokulsky *et al.* (2019) to discriminate between significant tornadoes and weaker events. Both studies showed the efficiency of this composite parameter in discriminating between (E)F0/(E)F1 and (E)F2+ cases. As shown in Figure 6c,d, both the (E)F0 and (E)F1 categories exhibit similar WMAXSHEAR₀₆, presenting smaller values for the SW than for the NE as a consequence of the lower CAPE. Significant tornadic events are usually associated with higher WMAXSHEAR₀₆, which is significantly different to that of the weak cases ($p < .030$), except that between the (E)F1 and (E)F2+ cases for the SW.

Chernokulsky *et al.* (2019) proposed the threshold of $940 \text{ m}^2\text{-s}^{-2}$ to distinguish between significant and weak tornadic environments. This value is too high for the SW events in our study (only 36% surpass it) and for those analysed in Taszarek *et al.* (2017), where less than 25% surpassed this threshold. The strong dependence of this parameter on CAPE, which is generally lower in the SW than in the NE, and the weak differences in the WS₀₆ between the SW and NE (E)F2+ events are the reasons for the lower WMAXSHEAR₀₆ among the SW events. In addition, the similar WS₀₆ of the (E)F1 and (E)F2+ cases in the SW subregion makes WMAXSHEAR₀₆ less useful in discriminating between significant and weak tornadic events in high-shear, low-CAPE environments. By contrast, 63% of the NE (E)F2+ events surpass the above-mentioned threshold.

To increase the difference in the WMAXSHEAR between the weak and significant tornadic events in HSLC environments, WS₀₃ instead of WS₀₆ has been proposed for the calculation of this parameter. Whereas the WS₀₃ presents significant differences between weak (grouping the (E)F0 and (E)F1 categories, not shown) and significant events for both the NE and SW subregions, the differences in the WS₀₆ between these vertical profile types are not statistically significant for the SW events.

Using WS₀₃, the differences in the WMAXSHEAR between the (E)F0, (E)F1 and WAT events with respect to (E)F2+ tornadoes are statistically significant for both the NE and SW subregions (Figure 6e,f). Although the 50th percentile for significant events is greater for the NE than the SW events, the KS-test results show that the distributions are not different, even for the other tornado categories (Table B2). Therefore, WMAXSHEAR₀₃, like the UTI, is unaffected by seasonal variations, that is, the

TABLE 3 WMAXSHEAR₀₃ 25th, 50th and 75th percentiles (in $\text{m}^2\text{-s}^{-2}$) for weak ((E)F0 and (E)F1) and significant ((E)F2+) events, merging NE and SW subregions

Percentile	Weak	Significant
P25	231	531
P50	380	811
P75	575	1,117

ability to distinguish between the tornado categories is invariant with seasonal changes.

Interestingly, the 25th percentile for WMAXSHEAR₀₃ of all the (E)F2+ soundings ($500 \text{ m}^2\text{-s}^{-2}$) is comparable to the 75th percentile of the weak tornado environments (Table 3). Therefore, this value could act as a threshold to distinguish between significant and weak tornado environments. Whereas only 29% of the (E)F0 cases and 35% of the (E)F1 events surpass this threshold, 84% of the (E)F2+ events exceed it.

3.3.3 | CAPE versus WS₀₃

The results from the previous sections indicate that SW tornadic events (more frequent during the cool-season) are usually associated with lower CAPE and higher helicity and WS than the NE events. Sherburn and Parker (2014) defined the criteria for HSLC environments as surface-based parcel CAPE $\leq 500 \text{ J-kg}^{-1}$, most-unstable parcel CAPE $\leq 1,000 \text{ J-kg}^{-1}$, and WS₀₆ $\geq 18 \text{ m-s}^{-1}$. In our study, 45% of the SW tornadoes meet these conditions compared to only 15% of the NE tornadoes (Table 2). This is consistent with the fact that cool-season severe weather events, including tornadoes, are usually associated with HSLC environments, as found in previous studies (Hanstrum *et al.*, 2002; Childs *et al.*, 2018; Gatzen *et al.*, 2019; Celiński-Mysław *et al.*, 2020).

Figure 7 shows the tornado and waterspout scatter plots of CAPE and WS₀₃ values overlaid onto WMAXSHEAR₀₃ contour lines. It is apparent that significant tornadoes associated with low CAPE are usually related to high WS₀₃, typically well above 15 m-s^{-1} . By contrast, when CAPE increases, significant tornadoes can occur even when WS₀₃ $< 15 \text{ m-s}^{-1}$. (E)F2+ events in the NE exhibit a wide range of CAPE and WS₀₃ values (Figure 7a), unlike the SW cases, which usually have CAPE $< 1,000 \text{ J-kg}^{-1}$ and WS₀₃ $> 15 \text{ m-s}^{-1}$ and only occasionally present high-CAPE and low-to-moderate WS₀₃ conditions (Figure 7b). Despite this apparent inverse correlation between CAPE and WS₀₃, as stated in Section 3.2.2, more than 75% of significant events from both subregions exhibit WMAXSHEAR₀₃ $> 500 \text{ m}^2\text{-s}^{-2}$.

FIGURE 7 NE (a) and SW (b) tornado and waterspout CAPE versus WS_{03} scatter plots overlaid with $WMAXSHEAR_{03}$ contour lines (labels expressed in $m^2 \cdot s^{-2}$).

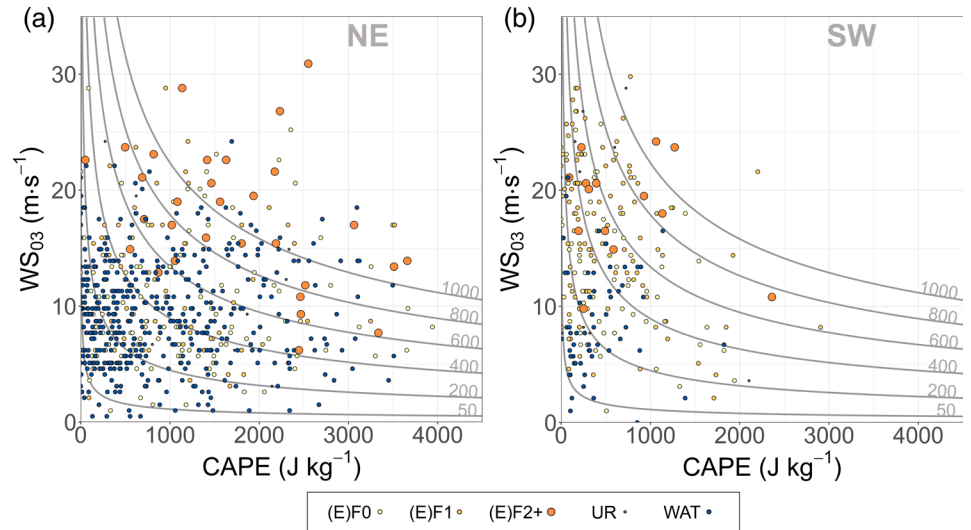
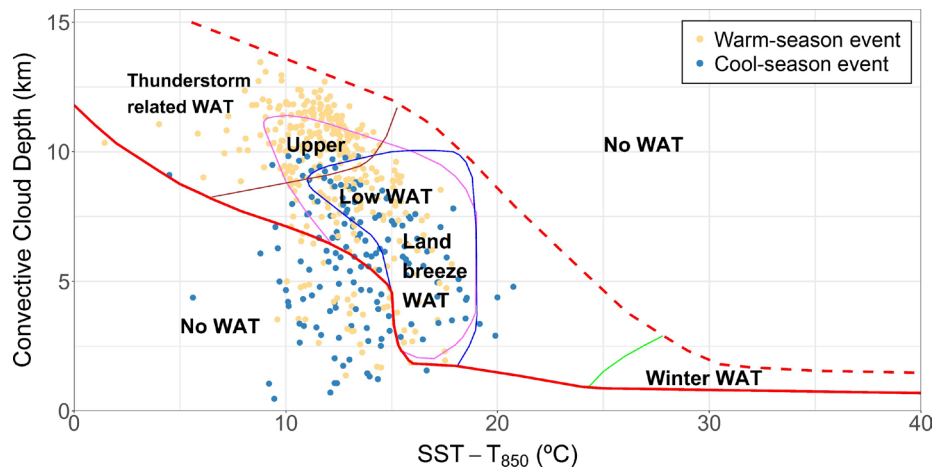


FIGURE 8 Szilagyi Waterspout Nomogram, where waterspout events are plotted according to the difference between the sea surface temperature (SST) and 850 hPa temperature (T_{850}), and the convective cloud depth (CCD), which is the difference between equilibrium level (EL) and lifting condensation level (LCL).



WAT and (E)F0 events are less restrictive than EF1+ events and are therefore associated with a wide range of CAPE and WS. However, they are more common when $CAPE < 1,500 J \cdot kg^{-1}$ and WS_{03} is around $10 m \cdot s^{-1}$ or even less, presenting $WMAXSHEAR_{03}$ smaller than $500 m^2 \cdot s^{-2}$.

3.3.4 | Szilagyi Waterspout Nomogram

The Szilagyi Waterspout Nomogram (Szilagyi, 2009) is an empirical graphical technique used to forecast waterspouts that was originally developed in the Great Lakes region of North America. It is based on two thermodynamic parameters: the difference between the SST and T_{850} (x -axis, ΔT) and the CCD (y -axis). Additionally, the 850 hPa wind speed must be lower than 40 kt ($20.6 m \cdot s^{-1}$). Depending on the ΔT and CCD, the nomogram classifies events into two broad areas: favourable conditions for waterspout formation (distinguishing four environments, that is, thunder-related, upper-low, land-

breeze and winter waterspouts; Figure 8) and unfavourable conditions (labelled 'No WAT' in Figure 8). According to Szilagyi (2009), the area of favourable conditions is limited by two threshold lines (thick-solid and thick-dashed lines in Figure 8), which are the upper and lower boundaries of the two areas of unfavourable conditions for waterspout formation.

We found that 81% of WAT events from the analysed dataset fit in the area where waterspout conditions are favourable. Here, the vast majority of warm-season events are associated with thunderstorm-related waterspout environments, similar to that reported by Keul *et al.* (2009). They are characterized by deep convective clouds (CCD exceeding 8.5 km) and low-to-moderate ΔT (below $16^\circ C$).

Unsurprisingly, the so-called winter waterspout conditions in the Szilagyi nomogram (Winter WAT in Figure 8), characterized by a high ΔT and low CCD, are not met in the study region, which is consistent with the findings of previous studies using the nomogram in other

parts of the Mediterranean (Sioutas *et al.*, 2013; Renko *et al.*, 2016). In our dataset, there was no waterspout case where $\Delta T > 25^\circ\text{C}$, with only two cases exceeding 20°C . It should be noted that this forecasting method was developed for the Great Lakes, where very cold low- and mid-level air advections in winter are common and, therefore, the difference between the surface temperature of the lake and T850 can reach large values. By contrast, in the Mediterranean basin and the south-western European Atlantic slope, cold air advections are weaker than at higher latitudes; thus, the ΔT in winter is not so extreme (Chandra *et al.*, 1990; Reynolds and Smith, 1995). In this sense, Keul *et al.* (2009) proposed a modification of the nomogram, excluding winter events where $\Delta T > 20^\circ\text{C}$ for the Mediterranean.

Most waterspout events that are not in the nomogram area of favourable conditions are characterized by a CCD between 1.5 and 6 km and a ΔT between 10 and 15°C . Of these, 63% are related to cool-season events, which are consistent with previous findings (Renko *et al.*, 2018) that have detected some winter Mediterranean waterspouts in this area of the nomogram. Therefore, this region should also be considered a potential area that is prone to mid-latitude winter waterspouts. Hence, the original nomogram should be modified when used for studies in southern Europe.

Apart from cool-season cases, the nomogram is a reliable source to identify conditions that are favourable for waterspouts in the study region. However, as pointed out by Szilagyi (2009), the nomogram is a complementary tool that should be used alongside the identification of additional factors such as lateral boundaries, frontal surfaces or low-level convergence lines. All of these can produce horizontal WS and generate low-level vertical vorticity, which can be stretched by updrafts, favouring waterspout formation (Brady and Szoke, 1989; Markowski and Richardson, 2009; Miglietta, 2019).

4 | SUMMARY AND CONCLUSIONS

A dataset including 907 tornado and waterspout events recorded from 1980 to 2018 in the Iberian Peninsula and Balearic Islands was analysed. Events were grouped depending on their intensity and type, with five categories considered ((E)F0, (E)F1, (E)F2+, UR and WAT). Data on the vertical temperature, dew point and wind profile of each event were retrieved from the ERA5 reanalysis. Thermodynamic (CAPE and CIN), kinematic (SRH and WS) and composite (UTI, WMAXSHEAR and the relationship between CAPE and WS_{03}) sounding-derived parameters were determined to characterize convective environments. Moreover, the Szilagyi Waterspout

Nomogram was tested for waterspout events in the dataset. We observed that there are substantial differences in the monthly distributions of tornadoes and waterspouts between the NE and SW parts of the study region. The events are more common during the warm-season (May to October) in the NE and during the cool-season (November to April) in the SW.

The NE tornado and waterspout environments are characterized by higher CAPE and lower WS and helicity (especially at low levels) compared to the SW events. In fact, 44% of the SW tornado atmospheric profiles are associated with high-shear, low-CAPE environments, in contrast to 13% for the NE events. Low-shear, high-LCL tornado environments occur in both areas, being more frequent inland during the warm-season. For this reason, they are more common in the NE (13% of the tornado events) than in the SW (6%).

There is a positive correlation between helicity and WS with respect to the intensity of the event. Generally, the higher the SRH and WS, the stronger the tornadoes can be. The majority of the (E)F2+ soundings in our dataset exceed the thresholds proposed by previous studies for significant tornadoes: $\text{SRH}_{03} > 180 \text{ m}^2\text{-s}^{-2}$ (57%); $\text{SRH}_{01} > 70 \text{ m}^2\text{-s}^{-2}$ (64%); $\text{WS}_{06} > 20 \text{ m-s}^{-1}$ (66%); $\text{WS}_{03} > 15 \text{ m-s}^{-1}$ (75%); and $\text{WS}_{01} > 8 \text{ m-s}^{-1}$ (52%). Moreover, the ratio of threshold exceedance is higher for the SW events than for the NE cases due to differences in the monthly distribution.

There is a weak inverse correlation between CAPE and WS_{03} . Whereas significant tornado environments with low CAPE ($< 1,000 \text{ J-kg}^{-1}$) usually present $\text{WS}_{03} > 15 \text{ m-s}^{-1}$, increasing CAPE makes it possible for EF2+ tornadoes to occur with smaller WS_{03} . This behaviour is similar for all the tornado and WAT categories.

Composite parameters such as the UTI (> 0.3) and WMAXSHEAR_{06} ($> 940 \text{ m}^2\text{-s}^{-2}$) are also generally good discriminators between weak and significant tornadoes. However, the WMAXSHEAR_{06} for SW (E)F2+ events is not as high as that for the NE ones due to the lower CAPE. Furthermore, the differences between the (E)F0/(E)F1 and (E)F2+ tornadoes are not statistically significant, making this parameter less useful in identifying significant tornado environments in HSLC conditions. This led us to apply a variant of WMAXSHEAR that uses WS_{03} instead of WS_{06} , and presents greater differences between the significant and weak tornadoes. Our results, which are also consistent with the inverse correlation between CAPE and WS_{03} , show that (E)F2+ environments are usually associated with $\text{WMAXSHEAR}_{03} > 500 \text{ m}^2\text{-s}^{-2}$. In this study, 80% of the significant tornado cases exceed this threshold, whereas only 29% of the weak tornadoes surpass it.

Neither the UTI nor WMAXSHEAR₀₃ presents significant differences between the NE and SW subregions for each category. This makes them useful in distinguishing between significant and weak tornado events, independently of their association with HSLC environments. However, there are some limitations in using the UTI for LHHCL environments as, according to its definition, the UTI is zero when LCL > 1,500 m, which often occurs in LHHCL cases.

It is remarkable that the UR and weak tornado events have similar values in the NE, while the UR and significant tornado events have comparable values for the kinematic parameters and UTI in the SW. This indicates that the UR events could be mostly weak in the NE, while some of the UR tornado cases might be significant in the SW.

By contrast, WAT are associated with low-to-moderate CAPE and low helicity and shear. Composite parameters also present low values for WAT compared to tornadoes, even the weak ones. Thus, the environmental conditions for waterspout formation are less restrictive than those for the formation of inland tornadoes.

The Szilagyi Waterspout Nomogram is a useful tool for forecasting waterspouts in our study area. The vast majority of the events (81%) fit into the nomogram area delimited by waterspout threshold lines, most of them being characterized by CCD > 8.5 km and $\Delta T < 16^\circ\text{C}$. However, the nomogram could be adapted to mid-latitudes by removing the $\Delta T > 25^\circ\text{C}$ winter waterspout area, as already discussed in previous studies, and defining a new cool-season waterspout area, with the CCD between 1.5 and 6 km and the ΔT between 10 and 15°C .

Our results might have been improved if the tornadic database used could distinguish between mesocyclonic and non-mesocyclonic cases. Therefore, future work should include an analysis of radar data to assess the convective mode (e.g., multicell, supercell, mesoscale convective system) of tornadic storms (Smith *et al.*, 2012), preferably over a larger region (i.e., Europe). Our analysis should be replicated, but through classifying tornadic events according to the type of parent-convective system, similar to that of Grams *et al.* (2012) or Thompson *et al.* (2012, 2013) in the USA. Moreover, it would be useful to determine the ratio of mesocyclonic tornadoes in non-typical supercell environments (i.e., WS₀₆ smaller than $20\text{ m}\cdot\text{s}^{-1}$). Finally, the SRH for the 0–500 m layer could also be analysed, as this parameter has been reported to be good at distinguishing between tornadic and non-tornadic supercell environments (Coffer *et al.*, 2019).

ACKNOWLEDGEMENTS

We would like to thank Delia Gutiérrez (Spanish Meteorological Agency) and Ricard Ripoll (Meteorological Service

of Catalonia) for providing the tornado and waterspout data from the SINOBAS and XOM platforms, respectively. This study was carried out within the framework of the HYdrological cycle in the Mediterranean Experiment (HyMeX) programme and with partial support from the projects CGL 2015-65627-C3-2-R (MINECO/FEDER), CGL 2016-81828-REDT (AEI) and RTI 2018-098693-B643-C32 (AEI), and the Water Research Institute (IdRA) of the University of Barcelona.

ORCID

Oriol Rodríguez  <https://orcid.org/0000-0003-1893-9959>

Joan Bech  <https://orcid.org/0000-0003-3597-7439>

REFERENCES

- Agee, A. and Jones, E. (2009) Proposed conceptual taxonomy for proper identification and classification of tornado events. *Weather and Forecasting*, 24, 609–6017. <https://doi.org/10.1175/2008WAF2222163.1>.
- Allen, J.T., Karoly, D.J. and Walsh, K.J. (2014) Future Australian severe thunderstorm environments. Part II: the influence of a strongly warming climate on convective environments. *Journal of Climate*, 27, 3848–3868. <https://doi.org/10.1175/JCLI-D-13-00426.1>.
- Antonescu, B., Schultz, D.M., Holzer, A. and Groenemeijer, P. (2017) Tornadoes in Europe: an underestimated threat. *Bulletin of the American Meteorological Society*, 98, 713–728. <https://doi.org/10.1175/BAMS-D-16-0171.1>.
- Arús, J. (2018). *25 años de tornados en Cataluña (1992–2017). (25 years of tornadoes in Catalonia, in Spanish)*. Simposio Nacional de Predicción "Memorial Antonio Mestre". pp. 563–574. DOI: <https://doi.org/10.31978/639-19-010-0.563>.
- Bech, J., Pascual, R., Rigo, T., Pineda, N., López, J.M., Arús, J. and Gayà, M. (2007) An observational study of the 7 September 2005 Barcelona tornado outbreak. *Natural Hazards and Earth System Science*, 7, 129–139. <https://doi.org/10.5194/nhess-7-129-2007>.
- Bech, J., Pineda, N., Rigo, T., Aran, M., Amaro, J., Gayà, M., Arús, J., Montanyà, J. and van der Velde, O. (2011) A Mediterranean nocturnal heavy rainfall and tornadic event. Part I: overview, damage survey and radar analysis. *Atmospheric Research*, 100(4), 621–637. <https://doi.org/10.1016/j.atmosres.2010.12.024>.
- Belo-Pereira, M., Andrade, C. and Pinto, P. (2017) A long-lived tornado on 7 December 2010 in mainland Portugal. *Atmospheric Research*, 185, 202–215. <https://doi.org/10.1016/j.atmosres.2016.11.002>.
- Blumberg, W.G., Halbert, K.T., Supinie, T.A., Marsh, P.T., Thompson, R.L. and Hart, J.A. (2017) SHARPPy: an open-source sounding analysis toolkit for the atmospheric sciences. *Bulletin of the American Meteorological Society*, 98, 1625–1636. <https://doi.org/10.1175/BAMS-D-15-00309.1>.
- Brady, R.H. and Szoke, E.J. (1989) A case study of nonmesocyclone tornado development in Northeast Colorado: similarities to waterspout formation. *Monthly Weather Review*, 117(4), 843–856.
- Bunkers, M.J., Klimowski, B.A., Zeitler, J.W., Thompson, R.L. and Weisman, M.L. (2000) Predicting supercell motion using anew

- hodograph technique. *Weather and Forecasting*, 15, 61–79. [https://doi.org/10.1175/1520-0434\(2000\)015,0061:PSMUAN.2.0.CO;2](https://doi.org/10.1175/1520-0434(2000)015,0061:PSMUAN.2.0.CO;2).
- Celin, ski-Mystlaw, D., Palarz, A. and Taszarek, M. (2020) Climatology and atmospheric conditions associated with cool season bow echo storms in Poland. *Atmospheric Research*, 240, 104944. <https://doi.org/10.1016/j.atmosres.2020.104944>.
- Chandra, S., Fleming, E.L., Schoeberl, M.R. and Barnett, J.J. (1990) Monthly mean global climatology of temperature, wind, geopotential height and pressure for 0–120 km. *Advances in Space Research*, 10(6), 3–12. [https://doi.org/10.1016/0273-1177\(90\)90230-W](https://doi.org/10.1016/0273-1177(90)90230-W).
- Chernokulsky, A.V., Kurgansky, M.V. and Mokhov, I.I. (2019) On characteristic reanalysis-based values of convective instability indices for Northern Eurasia tornadoes. *IOP Conference Series: Earth and Environmental Science*, 231, 012012. <https://doi.org/10.1088/1755-1315/231/1/012012>.
- Childs, S.J., Schumacher, R.S. and Allen, J.T. (2018) Cold-season tornadoes: climatological and meteorological insights. *Weather and Forecasting*, 33, 671–691. <https://doi.org/10.1175/WAF-D-17-0120.1>.
- Coffer, B.E., Parker, M.D., Thompson, R.L., Smith, B.T. and Jewell, R.E. (2019) Using near-ground storm relative helicity in supercell tornado forecasting. *Weather and Forecasting*, 34(5), 1417–1435. <https://doi.org/10.1175/WAF-D-19-0115.1>.
- Copernicus Climate Change Service (C3S) (2017). *ERA5: fifth generation of ECMWF atmospheric reanalyses of the global climate*. Copernicus Climate Change Service Climate Data Store (CDS). <https://cds.climate.copernicus.eu/cdsapp#!/home>. [17 April 2019]. DOI: 10.24381/cds.adbb2d47.
- Craven, J.P. and Brooks, H.E. (2004) Baseline climatology of sounding derived parameters associated with deep, moist convection. *National Weather Digest*, 28(1), 13–24.
- Davies, J.M. (2006) Tornadoes in environments with small helicity and/or high LCL Heights. *Weather and Forecasting*, 21, 579–594. <https://doi.org/10.1175/WAF928.1>.
- Davies-Jones, R.P., Burgess, D., Foster, M. (1990). Test of Helicity as a Tornado Forecast Parameter. Preprints, *16th Conference on Severe Local Storms, Kananaskis Park, AB, Canada*. American Meteorological Society: 588–592.
- Davis, J.M. and Parker, M.D. (2014) Radar climatology of tornadic and nontornadic vortices in high-shear, low-CAPE environments in the mid-Atlantic and southeastern United States. *Weather and Forecasting*, 29, 828–853. <https://doi.org/10.1175/WAF-D-13-00127.1>.
- Devanas, A. and Stefanova, L. (2018) Statistical prediction of waterspout probability for the Florida keys. *Weather and Forecasting*, 33, 389–410. <https://doi.org/10.1175/WAF-D-17-0100.1>.
- Doswell, C.A. and Schultz, D.M. (2006) On the use of indices and parameters in forecasting severe storms. *Electronic Journal of Severe Storms Meteorology*, 1(3), 1–22.
- Doswell, C.A., III, Brooks, H.E. and Dotzek, N. (2009) On the implementation of the enhanced Fujita scale in the USA. *Atmospheric Research*, 93(1–3), 554–563. <https://doi.org/10.1016/j.atmosres.2008.11.003>.
- Doswell, C.A., III and Rasmussen, E.N. (1994) The effect of neglecting the virtual temperature correction on CAPE calculations. *Weather and Forecasting*, 9, 625–629. [https://doi.org/10.1175/1520-0434\(1994\)009<0625:TEONTV>2.0.CO;2](https://doi.org/10.1175/1520-0434(1994)009<0625:TEONTV>2.0.CO;2).
- Dotzek, N., Groenemeijer, P., Feuerstein, B. and Holzer, A.M. (2009) Overview of ESSL's severe convective storms research using the European severe weather database ESWD. *Atmospheric Research*, 93(1–3), 575–586. <https://doi.org/10.1016/j.atmosres.2008.10.020>.
- Dowell, D.C. and Bluestein, H.B. (2002) The 8 June 1995 McLean, Texas, storm. Part I: observations of cyclic tornadogenesis. *Monthly Weather Review*, 130(11), 2626–2648. [https://doi.org/10.1175/1520-0493\(2002\)130<2626:TJMTSP>2.0.CO;2](https://doi.org/10.1175/1520-0493(2002)130<2626:TJMTSP>2.0.CO;2).
- Fujita, T.T. (1971). *Proposed characterization of tornadoes and hurricanes by area and intensity*. SMRP res. pap., University of Chicago, 91, 42 pp.
- Gall, M., Borden, K.A. and Cutter, S.L. (2008) When do losses count? Six fallacies of natural hazards loss data. *Bulletin of the American Meteorological Society*, 90, 799–810. <https://doi.org/10.1175/2008BAMS2721.1>.
- Gatzen, C.P., Fink, A.H., Schultz, D.M. and Pinto, J.G. (2019) An 18-year climatology of derechos in Germany. *Natural Hazards and Earth System Sciences*, 20(5), 1335–1351. <https://doi.org/10.5194/nhess-20-1335-2020>.
- Gayà, M. (2011) Tornadoes and severe storms in Spain. *Atmospheric Research*, 100(4), 334–343. <https://doi.org/10.1016/j.atmosres.2010.10.019>.
- Gayà, M. (2018) *Els Fiblons a Espanya: Climatologia i catàleg de Tornados i Trombes (Whirlwinds in Spain: Climatology and Catalogue of Tornadoes and Waterspouts, in Catalan)*, 2nd edition. Palma, Spain: Universitat de les Illes Balears 619 pp.
- Gayà, M., Homar, V., Romero, R. and Ramis, C. (2001) Tornadoes and waterspouts in the Balearic Islands: phenomena and environment characterization. *Atmospheric Research*, 56(1–4), 253–267. [https://doi.org/10.1016/S0169-8095\(00\)00076-4](https://doi.org/10.1016/S0169-8095(00)00076-4).
- Glickman, T.S. and Zenk, W. (2000) *Glossary of Meteorology*, 2nd edition. Boston, MA: American Meteorological Society 855 pp.
- Grams, J.S., Thompson, R.L., Snively, D.V., Prentice, J.A., Hodges, G.M. and Reames, L.J. (2012) A climatology and comparison of parameters for significant tornado events in the United States. *Weather and Forecasting*, 27, 106–123. <https://doi.org/10.1175/WAF-D-11-00008.1>.
- Groenemeijer, P., Púčik, T., Holzer, A.M., Antonescu, B., Riemann-Campe, K., Schultz, D.M., Kühne, T., Feuerstein, B., Brooks, H. E., Doswell, C.A., Koppert, H.J. and Sausen, R. (2017) Severe convective storms in Europe. Ten years of research and education at the European severe storms laboratory. *Bulletin of the American Meteorological Society*, 98, 2641–2651. <https://doi.org/10.1175/BAMS-D-16-0067.1>.
- Groenemeijer, P., Púčik, T., Tsonevsky, I., Bechtold, P. (2019). An overview of convective available potential energy and convective inhibition provided by NWP models for operational forecasting. *ECMWF Technical Memoranda*, 852. DOI: 10.21957/q392hofrl.
- Groenemeijer, P.H. and van Delden, A. (2007) Sounding-derived parameters associated with large hail and tornadoes in The Netherlands. *Atmospheric Research*, 83(2–4), 473–487. <https://doi.org/10.1016/j.atmosres.2005.08.006>.
- Grünwald, S. and Brooks, H.E. (2011) Relationship between sounding derived parameters and the strength of tornadoes in Europe and the USA from reanalysis data. *Atmospheric Research*, 100(4), 479–488. <https://doi.org/10.1016/j.atmosres.2010.11.011>.

- Gutiérrez, D., Riesco, J. and Ponce, S. (2015) SINOBAS, a tool for collaborative mapping applied to observation of “singular” weather phenomena. In: *15th EMS Annual Meeting & 12th European Conference on Applications of Meteorology (ECAM)*. Sofia, Bulgaria: European Meteorological Society.
- Hanstrum, B.N., Mills, G.A., Watson, A., Monteverdi, J.P. and Doswell, C.A. (2002) The cool-season tornadoes of California and southern Australia. *Weather and Forecasting*, 17, 705–722. [https://doi.org/10.1175/1520-0434\(2002\)017<0705:TCSTOC>2.0.CO;2](https://doi.org/10.1175/1520-0434(2002)017<0705:TCSTOC>2.0.CO;2).
- Hersbach, H., Bell, B., Berrisford, P., Hirahara, S., Horányi, A., Muñoz-Sabater, J., Nicolas, J., Peubey, C., Radu, R., Schepers, D., Simmons, A., Soci, C., Abdalla, S., Abellan, X., Balsamo, G., Bechtold, P., Biavati, G., Bidlot, J., Bonavita, M., Chiara, G., Dahlgren, P., Dee, D., Diamantakis, M., Dragani, R., Flemming, J., Forbes, R., Fuentes, M., Geer, A., Haimberger, L., Healy, S., Hogan, R.J., Hólm, E., Janisková, M., Keeley, S., Laloyaux, P., Lopez, P., Lupu, C., Radnoti, G., Rosnay, P., Rozum, I., Vamborg, F., Villaume, S. and Thépaut, J.N. (2020) The ERA5 global reanalysis. *Quarterly Journal of the Royal Meteorological Society*, 146, 1999–2049. <https://doi.org/10.1002/qj.3803>.
- Homar, V., Gayà, M., Romero, R., Ramis, C. and Alonso, S. (2003) Tornadoes over complex terrain: an analysis of the 28th August 1999 tornadic event in eastern Spain. *Atmospheric Research*, 67–68, 301–317. [https://doi.org/10.1016/S0169-8095\(03\)00064-4](https://doi.org/10.1016/S0169-8095(03)00064-4).
- Hyvärinen, O. and Saltikoff, E. (2010) Social media as a source of meteorological observations. *Monthly Weather Review*, 138(8), 3175–3184. <https://doi.org/10.1175/2010MWR3270.1>.
- Ingrosso, R., Lionello, P., Miglietta, M.M. and Salvadori, G. (2020) A statistical investigation of mesoscale precursors of significant tornadoes: the Italian case study. *Atmosphere*, 11(3), 301. <https://doi.org/10.3390/atmos11030301>.
- Jahn, M. (2015) Economics of extreme weather events: terminology and regional impact models. *Weather and Climate Extremes*, 10 (B), 29–39. <https://doi.org/10.1016/j.wace.2015.08.005>.
- Kahraman, A., Kadioglu, M. and Markowski, P.M. (2017) Severe convective storm environments in Turkey. *Monthly Weather Review*, 145, 4711–4725. <https://doi.org/10.1175/MWR-D-16-0338.1>.
- Kaltenböck, R., Diendorfer, G. and Dotzek, N. (2009) Evaluation of thunderstorm indices from ECMWF analyses, lightning data and severe storm reports. *Atmospheric Research*, 93(1–3), 381–396. <https://doi.org/10.1016/j.atmosres.2008.11.005>.
- Keul, A.G., Sioutas, M.V. and Szilagyi, W. (2009) Prognosis of central-eastern Mediterranean waterspouts. *Atmospheric Research*, 93(1–3), 426–436. <https://doi.org/10.1016/j.atmosres.2008.10.028>.
- Leit-ao, P. (2003) Tornadoes in Portugal. *Atmospheric Research*, 67, 381–390. [https://doi.org/10.1016/S0169-8095\(03\)00057-7](https://doi.org/10.1016/S0169-8095(03)00057-7).
- Maddox, R.A. (1976) An evaluation of tornado proximity wind and stability data. *Monthly Weather Review*, 104, 133–142. [https://doi.org/10.1175/1520-0493\(1976\)104<0133:AEOTPW>2.0.CO;2](https://doi.org/10.1175/1520-0493(1976)104<0133:AEOTPW>2.0.CO;2).
- Markowski, P.M. and Richardson, Y.P. (2009) Tornadogenesis: our current understanding, forecasting considerations, and questions to guide future research. *Atmospheric Research*, 93(1–3), 3–10. <https://doi.org/10.1016/j.atmosres.2008.09.015>.
- Matsangouras, I.T., Nastos, P.T., Bluestein, H.B., Pytharoulis, I., Papachristopoulou, K. and Miglietta, M.M. (2017) Analysis of waterspout environmental conditions and of parent-storm behaviour based on satellite data over the southern Aegean Sea of Greece. *International Journal of Climatology*, 37(2), 1022–1039. <https://doi.org/10.1002/joc.4757>.
- Miglietta, M.M. (2019). Waterspouts: a review. *Reference Module in Earth Systems and Environmental Sciences*. DOI: 10.1016/B978-0-12-409548-9.12414-5.
- Miglietta, M.M. and Matsangouras, I.T. (2018) An updated “climatology” of tornadoes and waterspouts in Italy. *International Journal of Climatology*, 38(9), 3667–3683. <https://doi.org/10.1002/joc.5526>.
- Miglietta, M.M., Mazon, J. and Rotunno, R. (2017) Numerical simulations of a tornadic supercell over the Mediterranean. *Weather and Forecasting*, 32, 1209–1226. <https://doi.org/10.1175/WAF-D-16-0223.1>.
- Moncrieff, M.W. and Miller, M.J. (1976) The dynamics and simulation of tropical cumulonimbus and squall lines. *Quarterly Journal Royal Meteorological Society*, 102, 373–394. <https://doi.org/10.1002/qj.49710243208>.
- Monteverdi, J.P., Doswell, C.A. and Lipari, G.S. (2003) Shear parameter thresholds for forecasting tornadic thunderstorms in northern and Central California. *Weather and Forecasting*, 18, 357–370. [https://doi.org/10.1175/1520-0434\(2003\)018<0357:SPTFFT>2.0.CO;2](https://doi.org/10.1175/1520-0434(2003)018<0357:SPTFFT>2.0.CO;2).
- Orlanski, I. (1975) A rational subdivision of scales for atmospheric processes. *Bulletin of the American Meteorological Society*, 56(5), 527–530.
- Potvin, C.K., Elmore, K.L. and Weiss, S.J. (2010) Assessing the impacts of proximity sounding criteria on the climatology of significant tornado environments. *Weather and Forecasting*, 25, 921–930. <https://doi.org/10.1175/2010WAF2222368.1>.
- Pučík, T., Groenemeijer, P., Rädler, A.T., Tijssen, L., Nikulin, G., Prein, A.F., van Meijgaard, E., Fealy, R., Jacob, D. and Teichmann, C. (2017) Future changes in European severe convection environments in a regional climate model ensemble. *Journal of Climate*, 30, 6771–6794. <https://doi.org/10.1175/JCLI-D-16-0777.1>.
- Pučík, T., Groenemeijer, P., Rýva, D. and Kolář, M. (2015) Proximity soundings of severe and nonsevere thunderstorms in Central Europe. *Monthly Weather Review*, 143, 4805–4821. <https://doi.org/10.1175/MWR-D-15-0104.1>.
- Quirantes, J.A., Riesco, J., Núñez, J.A. (2014). *Características básicas de las supercélulas en España (Supercell basic characteristics in Spain, in Spanish)*. AEMET - Publicaciones en línea. <http://hdl.handle.net/20.500.11765/709>.
- Ramis, C., Arús, J., López, J. and Mestres, A. (1997) Two cases of severe weather in Catalonia (Spain): an observational study. *Meteorological Applications*, 4(3), 207–217. <https://doi.org/10.1017/S1350482797000510>.
- Ramis, C., Romero, R. and Homar, V. (2009) The severe thunderstorm of 4 October 2007 in Mallorca: an observational study. *Natural Hazards and Earth System Sciences*, 9(4), 1237–1245. <https://doi.org/10.5194/nhess-9-1237-2009>.
- Rasmussen, E.N. (2003) Refined supercell and tornado forecast parameters. *Weather and Forecasting*, 18, 530–535. [https://doi.org/10.1175/1520-0434\(2003\)18<530:RSATFP>2.0.CO;2](https://doi.org/10.1175/1520-0434(2003)18<530:RSATFP>2.0.CO;2).
- Rasmussen, E.N. and Blanchard, D.O. (1998) A baseline climatology of sounding-derived supercell and tornado forecast parameters. *Weather and Forecasting*, 13, 1148–1164. [https://doi.org/10.1175/1520-0434\(1998\)013<1148:ABCOSD>2.0.CO;2](https://doi.org/10.1175/1520-0434(1998)013<1148:ABCOSD>2.0.CO;2).

- Renko, T., Ivušić, S., Prtenjak, M.T., Šoljan, V. and Horvat, I. (2018) Waterspout forecasting method over the eastern Adriatic using a high-resolution numerical weather model. *Pure and Applied Geophysics*, 175, 3759–3778. <https://doi.org/10.1007/s00024-018-1833-x>.
- Renko, T., Kuzmić, J., Šoljan, V. and Mahović, N.S. (2016) Waterspouts in the eastern Adriatic from 2001 to 2013. *Natural Hazards*, 82, 441–470. <https://doi.org/10.1007/s11069-016-2192-5>.
- Reynolds, R.W. and Smith, T.M. (1995) A high-resolution Global Sea surface temperature climatology. *Journal of Climate*, 8, 1571–1583. [https://doi.org/10.1175/1520-0442\(1995\)008<1571:AHRGSS>2.0.CO;2](https://doi.org/10.1175/1520-0442(1995)008<1571:AHRGSS>2.0.CO;2).
- Riemann-Campe, K., Fraedrich, K. and Lunkeit, F. (2009) Global climatology of convective available potential energy (CAPE) and convective inhibition (CIN) in ERA-40 reanalysis. *Atmospheric Research*, 93(1–3), 534–545. <https://doi.org/10.1016/j.atmosres.2008.09.037>.
- Riesco, J., Polvorinos, F., Núñez, J.A., Soriano, J.D. and Jiménez, C. (2015) *Climatología de tornados en España Peninsular y Baleares (Tornado Climatology in the Peninsular Spain and Balearic Islands, in Spanish)*. Madrid, Spain: Spanish Meteorological Agency (AEMet), 83 pp. Available at: http://www.aemet.es/documentos/es/conocermas/publicaciones/Climatologia_tornados/Climatologia_tornados.pdf [Accessed 27th February 2020].
- Ripoll, R., del Amo, X. and Vendrell, R. (2016) The weather observers network of the Meteorological Service of Catalonia. In: *In WMO Technical Conference on Meteorological and Environmental Instruments and Methods of Observation (CI-MO TECO)*. Spain, Madrid: World Meteorological Organization.
- Rodríguez, O. and Bech, J. (2018) Sounding-derived parameters associated with tornadic storms in Catalonia. *International Journal of Climatology*, 38, 2400–2414. <https://doi.org/10.1002/joc.5343>.
- Rodríguez, O. and Bech, J. (2020) Reanalysing strong-convective wind damage paths using high-resolution aerial images. *Natural Hazards*, 104, 1021–1038. <https://doi.org/10.1007/s11069-020-04202-6>.
- Rodríguez, O., Bech, J., Soriano, J.D., Gutiérrez, D. and Castán, S. (2020) A methodology to conduct wind damage field surveys for high-impact weather events of convective origin. *Natural Hazards and Earth System Science*, 20(5), 1513–1531. <https://doi.org/10.5194/nhess-20-1513-2020>.
- Romero, R., Gayà, M. and Doswell, C.A. (2007) European climatology of severe convective storm environmental parameters: a test for significant tornado events. *Atmospheric Research*, 83(2–4), 389–404. <https://doi.org/10.1016/j.atmosres.2005.06.011>.
- Sánchez-Laulhé, J.M. (2009) El tornado de Málaga del 1 de Febrero de 2009 (the Málaga tornado from 1 February 2009, in Spanish). *AME Boletín*, 24, 34–36.
- Seeley, J.T. and Romps, D.M. (2015) The effect of global warming on severe thunderstorms in the United States. *Journal of Climate*, 28, 2443–2458. <https://doi.org/10.1175/JCLI-D-14-00382.1>.
- Sherburn, K.D. and Parker, M.D. (2014) Climatology and ingredients of significant severe convection in high-shear, low-CAPE environments. *Weather and Forecasting*, 29, 854–877. <https://doi.org/10.1175/WAF-D-13-00041.1>.
- Sioutas, M., Szilagyi, W. and Keul, A. (2013) Waterspout outbreaks over areas of Europe and North America: environment and predictability. *Atmospheric Research*, 123, 167–179. <https://doi.org/10.1016/j.atmosres.2012.09.013>.
- Sioutas, M.V. and Keul, A.G. (2007) Waterspouts of the Adriatic, Ionian and Aegean Sea and their meteorological environment. *Atmospheric Research*, 83(2–4), 542–557. <https://doi.org/10.1016/j.atmosres.2005.08.009>.
- Smith, B.T., Thompson, R.L., Grams, J.S., Broyles, C. and Brooks, H.E. (2012) Convective modes for significant severe thunderstorms in the contiguous United States. Part I: storm classification and climatology. *Weather and Forecasting*, 27, 1114–1135. <https://doi.org/10.1175/WAF-D-11-00115.1>.
- Szilagyi, W. (2009) A waterspout forecasting technique. In: *5h European Conference on Severe Storms (ECSS)*. Landshut, Germany: European Severe Weather Laboratory. Available at: <https://www.essl.org/ECSS/2009/preprints/O05-14-szilagyi.pdf>. [Accessed 25th August 2020].
- Taszarek, M., Allen, J., Puciak, T., Groenemeijer, P., Czernecki, B., Kolendowicz, L., Lagouvardos, K., Kotroni, V. and Schulz, W. (2019) A climatology of thunderstorms across Europe from a synthesis of multiple data sources. *Journal of Climate*, 32, 1813–1837. <https://doi.org/10.1175/JCLI-D-18-0372.1>.
- Taszarek, M., Brooks, H.E. and Czernecki, B. (2017) Sounding-derived parameters associated with convective hazards in Europe. *Monthly Weather Review*, 145, 1511–1528. <https://doi.org/10.1175/MWR-D-16-0384.1>.
- Taszarek, M., Brooks, H.E., Czernecki, B., Szuster, P. and Fortuniak, K. (2018) Climatological aspects of convective parameters over Europe: a comparison of ERA-interim and sounding data. *Journal of Climate*, 31, 4281–4308. <https://doi.org/10.1175/JCLI-D-17-0596.1>.
- Taszarek, M. and Kolendowicz, L. (2013) Sounding-derived parameters associated with tornado occurrence in Poland and Universal Tornadic Index. *Atmospheric Research*, 134, 186–197. <https://doi.org/10.1016/j.atmosres.2013.07.016>.
- Thompson, R.L., Edwards, R., Hart, J.A., Elmore, K.L. and Markowski, P. (2003) Close proximity soundings within supercell environments obtained from the rapid update cycle. *Weather and Forecasting*, 18, 1243–1261. [https://doi.org/10.1175/1520-0434\(2003\)018<1243:CPSWSE>2.0.CO;2](https://doi.org/10.1175/1520-0434(2003)018<1243:CPSWSE>2.0.CO;2).
- Thompson, R.L., Smith, B.T., Dean, A.R. and Marsh, P.T. (2013) Spatial distributions of tornadic near-storm environments by convective mode. *Electronic Journal of Severe Storms Meteorology*, 8(5), 1–22.
- Thompson, R.L., Smith, B.T., Grams, J.S., Dean, A.R. and Broyles, C. (2012) Convective modes for significant severe thunderstorms in the contiguous United States. Part II: supercell and QLCS tornado environments. *Weather and Forecasting*, 27, 1136–1154. <https://doi.org/10.1175/WAF-D-11-00116.1>.
- Viceto, C., Marta-Almeida, M. and Rocha, A. (2017) Future climate change of stability indices for the Iberian Peninsula. *International Journal of Climatology*, 37(12), 4390–4408. <https://doi.org/10.1002/joc.5094>.
- Wade, A.R., Coniglio, M.C. and Ziegler, C.L. (2018) Comparison of near- and far-field supercell inflow environments using radiosonde observations. *Monthly Weather Review*, 146, 2403–2415. <https://doi.org/10.1175/MWR-D-17-0276.1>.
- Wakimoto, R.M., Atkins, N.T., Butler, K.M., Bluestein, H.B., Thiem, K., Snyder, J. and Houser, J. (2015) Photogrammetric analysis of the 2013 El Reno tornado combined with Mobile X-band Polarimetric radar data. *Monthly Weather Review*, 143, 2657–2683. <https://doi.org/10.1175/MWR-D-15-0034.1>.

Weisman, M.L. and Klemp, J.B. (1982) The dependence of numerically simulated convective storms on vertical wind shear and buoyancy. *Monthly Weather Review*, 110, 504–520. [https://doi.org/10.1175/1520-0493\(1982\)110<0504:TDONSC>2.0.CO;2](https://doi.org/10.1175/1520-0493(1982)110<0504:TDONSC>2.0.CO;2).

Weisman, M.L. and Rotunno, R. (2000) The use of vertical wind shear versus helicity in interpreting supercell dynamics. *Journal of the Atmospheric Sciences*, 57, 1452–1472. [https://doi.org/10.1175/1520-0469\(2000\)057<1452:TUOVWS>2.0.CO;2](https://doi.org/10.1175/1520-0469(2000)057<1452:TUOVWS>2.0.CO;2).

Weisman, M.L., Trapp, R.J., Romine, G.S., Davis, C., Torn, R., Baldwin, M., Bosart, L., Brown, J., Coniglio, M., Dowell, D., Evans, A.C., Galarneau, T.J., Haggerty, J., Hock, T., Manning, K., Roebber, P., Romashkin, P., Schumacher, R., Schwartz, C.S., Sobash, R., Stensrud, D. and Trier, S.B. (2015) The mesoscale predictability experiment (MPEX). *Bulletin of*

the American Meteorological Society, 96, 2127–2149. <https://doi.org/10.1175/BAMS-D-13-00281.1>.

WSEC. (2006) *A Recommendation for an Enhanced Fujita Scale (EF-scale)*. Lubbock, TX: Wind Science and Engineering Center 111 pp. Available at: <http://www.spc.noaa.gov/faq/tornado/EFScale.pdf>. [Accessed 4th March 2020].

APPENDIX A.

In this Appendix, the equations for all the parameters analysed are shown (Table A1).

TABLE A 1 Equation, units and reference for the parameters analysed. Variables used are g (acceleration of gravity), LFC (level of free convection), EL (equilibrium level), $T_{v,LP}$ (lifting parcel temperature), T_v (environmental temperature), h (height of the upper-limit of an air layer above ground level), v (horizontal wind vector), k (upward unit vector), c (storm motion vector), SBCAPE (surface-based CAPE), SBLCL (surface-based lifting condensation level), SBCAPE₀₃ (surface-based CAPE integrated up to 3 km) and AMR₅₀₀ (mixing ratio average in the lowest 500 m). Note that UTI is a dimensionless (d.l.) magnitude and that it is imposed that UTI = 0 if SBCAPE = 0 J·kg⁻¹ and/or LCL > 1,500 m, whereas if SRH₀₁ < 0 m²·s⁻², then it is considered that SRH₀₁ = 0 m²·s⁻²

Parameter	equation	Units	Reference
CAPE	$g \int_{LFC}^{EL} \frac{T_{v,LP} \partial z - T_v \partial z}{T_v \partial z} dz$	J·kg ⁻¹	Moncrieff and Miller (1976)
CIN	$g \int_0^{LFC} \frac{T_{v,LP} \partial z - T_v \partial z}{T_v \partial z} dz$	J·kg ⁻¹	Moncrieff and Miller (1976)
SRH ₀₁	$-\frac{\partial}{\partial t} \int_0^h k \cdot \delta v - c \cdot \frac{\partial v}{\partial z} dz$	m ² ·s ⁻²	Davies-Jones <i>et al.</i> (1990)
WS _{0h}	$\frac{1}{nh} \int_0^h jv_h - v_0j$	m·s ⁻¹	Weisman and Klemp (1982)
UTI	$\frac{SBCAPE - SRH_{01}}{200} + \frac{5 \delta WS_{06} + 20 \delta WS_{10} + \delta WS_{2000} - SBLCL}{100} + \frac{SRH_{01}}{10} + \frac{SBCAPE_{03}}{4} - \frac{WS_{01}}{12} - \frac{AMR_{500}}{10}$	d. l.	Taszarek and Kolendowicz (2013)
WMAXSHEAR ₀₁	$\frac{1000}{2} \sqrt{CAPE} \cdot WS_{01}$	m ² ·s ⁻²	Taszarek <i>et al.</i> (2017), this study

APPENDIX B.

Table B1 presents the results of the Kolmogorov–Smirnov (KS) test assessing the statistical significance of differences between the values of the analysed parameters in

relation to the event classes ((E)F0, (E)F1, (E)F2+, UR and WAT) for both subregions of the study (NE and SW). Table B2 shows the *p*-values of the KS-test performed to determine how different the distributions of each parameter are, comparing the NE and SW subregions.

TABLE B 1 *p*-values of the Kolmogorov–Smirnov test for all the parameters analysed for both NE and SW subregions, comparing among the different event classes. *p*-values over .100 are not shown and *p*-values equal to or lower than .010 are in bold

Parameter	(E)F0 vs. (E)F1	(E)F0 vs. (E)F2+	(E)F0 vs. UR	(E)F0 vs. WAT	(E)F1 vs. (E)F2+	(E)F1 vs. UR	(E)F1 vs. WAT	(E)F2+ vs. UR	(E)F2+ vs. WAT	UR vs. WAT
CAPE (NE)	–	.024	–	.012	.030	–	.038	–	.000	–
CAPE (SW)	–	–	–	–	–	–	–	–	–	–
CIN (NE)	–	–	–	–	–	–	–	–	–	–
CIN (SW)	–	–	–	–	–	–	–	–	–	–
SRH ₀₃ (NE)	.045	.000	–	–	.027	–	.000	–	.000	–
SRH ₀₃ (SW)	.001	.005	.070	.002	–	–	.000	–	.000	.006
SRH ₀₁ (NE)	.001	.001	–	.055	–	–	.000	–	.000	.066
SRH ₀₁ (SW)	.001	.003	–	.001	–	–	.000	–	.000	.017
WS ₀₆ (NE)	–	.001	–	–	.001	–	–	–	.000	–
WS ₀₆ (SW)	.001	.006	–	.023	–	–	.000	–	.000	.086
WS ₀₃ (NE)	.059	.000	–	–	.002	–	.001	.076	.000	–
WS ₀₃ (SW)	.003	.007	.056	.003	–	–	.000	–	.000	.006
WS ₀₁ (NE)	.018	.021	–	.018	–	–	.000	–	.000	–
WS ₀₁ (SW)	.000	.026	.084	.003	–	–	.000	–	.000	.006
UTI (NE)	.005	.000	–	.016	.013	–	.000	.047	.000	–
UTI (SW)	.074	.010	–	.006	–	–	.000	–	.000	–
WMAXSHEAR ₀₆ (NE)	–	.000	–	.006	.000	–	.001	.021	.000	.018
WMAXSHEAR ₀₆ (SW)	.053	.029	–	.069	–	–	.000	.076	.000	–
WMAXSHEAR ₀₃ (NE)	.100	.000	–	.018	.000	–	.000	.012	.000	–
WMAXSHEAR ₀₃ (SW)	–	.006	–	.002	.030	–	.000	–	.000	–

Parameter	(E)F0	(E)F1	(E)F2+	UR	WAT
CAPE	.000	.000	.002	–	.000
CIN	–	–	–	–	–
SRH ₀₃	.002	.003	–	–	–
SRH ₀₁	.000	.000	.007	–	.008
WS ₀₆	.047	.000	–	–	–
WS ₀₃	.022	.000	–	–	–
WS ₀₁	.000	.000	.012	–	.002
UTI	.035	–	–	–	–
WMAXSHEAR ₀₆	.097	.055	.018	–	.025
WMAXSHEAR ₀₃	–	–	–	–	.022

TABLE B 2 As Table B1 but for *p*-values of the Kolmogorov–Smirnov test for each parameter analysed, comparing NE and SW values distribution

APPENDIX C.

Tornadic events recorded in Catalonia between 2000 and 2016, which are included in the dataset used in this study, are analysed in this Appendix. ERA5 reanalysis data and real sounding observations previously used in RB18 are compared. In RB18, pre-convective environments were analysed by selecting the most representative sounding for each event, using the proximity-inflow method (Rasmussen and Blanchard, 1998). Values of the thermodynamic (CAPE), kinematic (WS_{03}) and composite (WMAXSHEAR₀₃) parameters from both datasets are presented and compared

Table C1 shows some of the differences in the 25th, 50th and 75th percentiles. CAPE ERA5 values are generally higher than those derived from the sounding data, except for the upper bound. This is consistent with the findings of Potvin *et al.* (2010), who reported that increasing the

spatio-temporal distance between the sounding data and the tornadic event analysed produced lower CAPE environments. By contrast, reanalysis-derived WS_{03} and WMAXSHEAR₀₃ percentiles are similar or slightly lower than those derived from soundings. These differences could be explained by the:

- *Data used:* Here, ERA5 reanalysis data are employed, whereas real sounding data were used in RB18 (see Taszarek *et al.*, 2018 for further details on this issue).
- *Profile selection method:* We selected the closest spatio-temporal grid point to analyse convective environments, whereas the proximity-inflow method was used in RB18 (profiles could be at ranges farther than 200 km and several hours earlier than the event).

In any case, all these differences are not statistically significant ($p > .200$, according to the KS test, not shown).

TABLE C 1 25th, 50th and 75th percentiles for CAPE, WS_{03} and WMAXSHEAR₀₃ for ERA5 (in bold, left columns) and radiosounding (right columns) data for (E)F0, (E)F1+ and WAT Catalonia (2000–2016) events analysed in Rodriguez and Bech (2018)

	(E)F0		(E)F1+		WAT	
CAPE ($J\cdot kg^{-1}$)						
P25	429	266	492	478	330	224
P50	766	757	1,018	702	669	539
P75	1,367	1,609	1,359	1701	1,350	1,209
WS_{03} ($m\cdot s^{-1}$)						
P25	6.6	7.9	9.4	12.9	6.7	6.5
P50	9.8	11.8	14.7	16.0	9.8	9.0
P75	13.4	14.0	21.2	18.5	12.9	13.2
WMAXSHEAR ₀₃ ($m^2\cdot s^{-2}$)						
P25	156	255	394	437	167	147
P50	354	389	483	527	331	283
P75	461	744	841	830	573	517